Microchimica Acta (2022) 189: 83
https://doi.org/10.1007/s00604-021-05153-w

REVIEW ARTICLE

Conjugated polymer nanoparticles and their nanohybrids as smart photoluminescent and photoresponsive material for biosensing, imaging, and theranostics

Xi Chen[1] · Sameer Hussain[1] · Ansar Abbas[1] · Yi Hao[2] · Akhtar H. Malik[3] · Xuemeng Tian[1] · Huijia Song[4] · Ruixia Gao[1]

Received: 23 August 2021 / Accepted: 13 December 2021 / Published online: 3 February 2022

Abstract

The emergence of conjugated polymers (CPs) has provided a pathway to attain smart multifunctional conjugated polymer nanoparticles (CPNs) with enhanced properties and diverse applications. CPNs based on π-extended CPs exhibit high fluorescence brightness, low cytotoxicity, excellent photostability, reactive oxygen species (ROS) generation ability, high photothermal conversion efficiency (PCE), etc. which endorse them as an excellent theranostic tool. Furthermore, the unique light-harvesting and energy transfer properties of CPNs enables their transformation into smart functional nanohybrids with augmented performance. Owing to such numerous features, simple preparation method and an easy separation process, the CPNs and their hybrids have been constantly rising as a frontrunner in the domain of medicine and much work has been done in the respective research area. This review summarizes the recent progress that has been made in the field of CPNs for biological and biomedical applications with special emphasis on biosensing, imaging, and theranostics. Following an introduction into the field, a first large section provides overview of the conventional as well as recently established synthetic methods for various types of CPNs. Then, the CPNs-based fluorometric assays for biomolecules based on different detection strategies have been described. Later on, examples of CPNs-based probes for imaging, both in vitro and in vivo using cancer cells and animal models have been explored. The next section highlighted the vital theranostic applications of CPNs and corresponding nanohybrids, mainly via imaging-guided photodynamic therapy (PDT), photothermal therapy (PTT) and drug delivery. The last section summarizes the current challenges and gives an outlook on the potential future trends on CPNs as advanced healthcare material.

Keywords Conjugated polymer nanoparticles (CPNs) · Nanohybrids · Biosensing · Fluorometric assay · Imaging · Theranostic application · Phototherapy · Drug delivery

Introduction

Conjugated polymers (CPs, also known as semiconducting polymers), as a kind of superior conducting material, have attracted profound interest in the fabrication of optoelectronic devices owing to their excellent electrical features. Since the Nobel Prize-winning research on highly conductive polyacetylene in the 1970s [1], significant advancements have been made in both the designing as well as application of CP materials. Later, the CPs were also discovered to exhibit remarkable optical properties which further broaden their prospects in the area of sensing, imaging, and diagnosis. Due to their unique signal-amplification properties, they are considered as promising and found multiple applications in trace detection of analytes, biomedical imaging, and phototherapy [2–7]. Thus, the past decades have witnessed

Xi Chen and Sameer Hussain contributed equally to the work.

✉ Sameer Hussain
sameer@xjtu.edu.cn

✉ Ruixia Gao
ruixiagao@xjtu.edu.cn

1 School of Chemistry, Xi'an Jiaotong University, Xi'an 710049, Shaanxi, China

2 School of Pharmacy, Health Science Center, Xi'an Jiaotong University, Xi'an 710061, Shaanxi, China

3 Department of Chemistry, Government Degree College, Sopore 193201, Jammu & Kashmir, India

4 Department of Urology, Second Affiliated Hospital of Xi'an Jiaotong University, Xi'an 710004, Shaanxi, China

numerous CPs as advanced functional materials [8–13] to fabricate solar cells, light-emitting diodes and high-performance probes for a variety of biomedical applications.

Although the CPs have received considerable interest in the field of detection, their further application in biomedical science is still limited due to their poor solubility in water, relatively high cytotoxicity, less photostability, difficulty in separation and complex purification steps. To overcome the existing limitations, conjugated polymer nanoparticles (CPNs) derived from CPs have emerged as smart optical material that combines the properties of signal amplified CPs and the conventional nanoparticles [14, 15]. Owing to their augmented properties in aqueous media including large absorption cross-section, high brightness, flexible surface modification, good photostability and ease of separation, CPNs are considered as revolutionary material in the area of theranostics [16]. Shu Wang's research group [17, 18] elegantly described the superiority and unique advantages of CPNs over other materials for biological applications. Owing to unique signal amplification property [19] and other vital features, CPNs has become an auspicious material in the fields of drug/gene delivery [20], tumor imaging [21], and biomolecular detection [22, 23]. The properties and functions of CPNs varied with size [24], dispersion and packing of the particles in the lattice, which can be systematically controlled by the molecular designing or changing the preparation method. Thus, based on size, morphology and colloidal stability, the CPNs can be classified into various forms like conjugated polymer dots (Pdots) [25], nanofibres [26], nanocomposites and core–shell structures [27].

In recent years, a significant number of CPNs and their hybrids for biomedical applications have been developed and reported by scientists working in the multidisciplinary areas of chemistry, medicine and biology. In 2014, Hao's research group [28] summarized the advances on development of electrochemical sensors using nanocomposites of conducting polymers with graphene. The review highlighted the application of such conductive composite materials in chemo- and biosensing owing to their superior electrical, chemical, structural and thermal properties. In 2018, Zheng et al. [29] highlighted the applications of CPNs in near-infrared II (NIR-II) imaging and therapy. A recent review by Manners et al. [30] provide an overview of the advanced methods used to prepare CPNs with special emphasis on newly established "self-assembly" and "microfluidic method" for potential application in multiple areas. In 2021, Dalkiran and Brett [31] described the recent developments in the area of electrochemical (bio)sensing using combination of polyphenazine/polytriphenylmethane redox polymers with semiconductor nanoparticles. Considering progressive developments, it is necessary to highlight the latest advancements related to CPNs in the field of healthcare. In continuation to previous efforts [18, 25, 32] of collecting the fascinating research on CPNs, we hereby provide some recent advances of CPNs as photoluminescent and photoresponsive materials in biosensing, imaging, and theranostics (Fig. 1). The review begins with a description of the conventional and modern synthetic methods used for the preparation of various types of CPNs. Then, the application of CPNs in biosensing using different mechanisms has been summarized which revealed the detection and estimation of some important biomolecules. Following this, the diagnosis of diseases mainly cancer via in-vitro and in-vivo imaging has been described. Next, the theranostic applications of CPNs via imaging-guided phototherapy and drug delivery have been explored taking representative examples. Finally, the future prospects, as well as the obstacles that stand in the way of further progress have been highlighted thoroughly.

Methods of preparation

CPs are the main components of CPNs which determine their optical property. Thus, the synthesis of CPs with a suitable backbone structure is the first step towards the fabrication of CPNs. After the synthesis of CPs, they are converted into corresponding CPNs through various fabrication methods which control the size, morphology and stability of CPNs. This section briefly introduces some popular methods of synthesizing CPs and provides comprehensive discussion on fabrication procedures of the various types of CPNs.

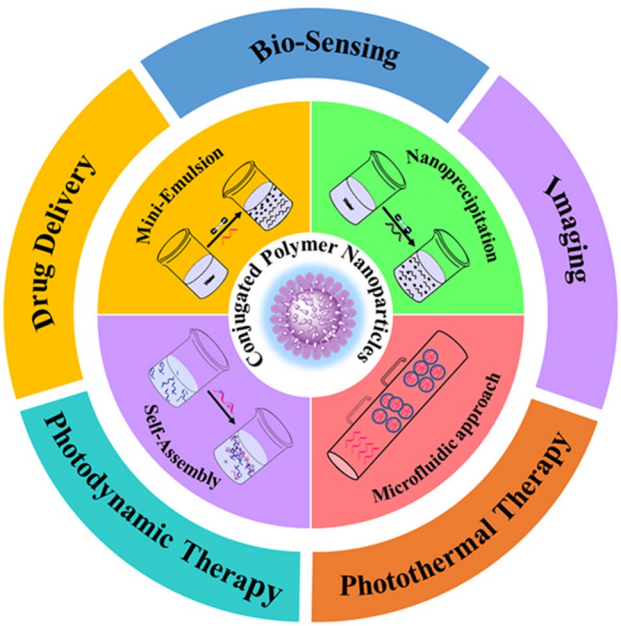

Fig. 1 Overview of the most common synthetic methods of CPNs and their biological applications

Synthesis of CPs

The CPs are organic macromolecules which composed of π-conjugated backbone of alternate single and double bonds that regulate its optoelectrical properties [33, 34]. On the basis of variable backbone structure, the CPs be classified as, poly(fluorene-co-phenylene) (PFP), poly(p-phenylene vinylene) (PPV), poly(p-phenylene) (PPP), polypyrrole (PPy), polyfluorene (PF), polythiophene (PT), polydiacetylene (PDA), poly(p-phenylene ethynylene) (PPE), etc. The most common polymerization techniques for synthesizing CPs include palladium-catalyzed coupling reaction (Suzuki [35], Heck [36], and Sonogashira [37]), oxidative polymerization and Stille coupling [38]. Thus, the CPs with different backbone structures can be attained by employing appropriate synthetic methods.

Fabrication of CPNs

CPNs can be fabricated by various techniques to obtain nanoparticles of desire characteristics such as size, structure and stability. While, mini-emulsion and nanoprecipitation represents frequently used methods of acquiring CPNs, the latest techniques include microfluidic approach and self-assembly. Kelly and Wolf [27] provide another interesting approach to classify CPNs based on their method of preparation using "soft" or "hard" templates. CPNs prepared using soft-templates usually get deformed easily and exhibit structural persistency only in solution state. Emulsion, reprecipitation and emulsion-dispersion polymerization methods which constitute surfactants are common examples of soft-template approaches. Besides, the hard-templates based CPNs exhibit features of persistent shape with structural stability both in solution as well as solid state. CPNs with core–shell structures and silica nanocomposites are usually acquired using hard template method. The brief descriptions of these vital methods are given below.

Mini-emulsion method

In the mini-emulsion method, the CPNs are prepared usually by adding surfactant to avoid emulsion droplet aggregation. Briefly, the CPs dissolved in an apolar solvent like dichloromethane (DCM) are added into the aqueous solution containing surfactant molecules, and then the organic phase is uniformly dispersed in the water phase by ultrasonic treatment to form a homogenous emulsion. Lastly, CPNs are obtained by after evaporating the organic solvent (Fig. 2a). Prior to this method, it was a difficult and time-consuming task to chemically modify the formed nanoparticles with specific functional groups. The mini-emulsion method exhibits the advantage that surfactants can migrate or adsorb directly onto the framework of CPs [39]. Liu and co-workers reported different CPNs with emission covering the whole visible light range by co-encapsulating poly(D-L-lactide-co-glycolide) (PLGA) [40]. In this protocol, small quantity CP and PLGA dissolved in DCM was added to excess water with poly(vinylalcohol) (PVA) as an emulsifier. Then, the CPNs were obtained by ultrasonication followed by evaporation of the organic solvents. This improved solvent evaporation single emulsion method with PVA as emulsifier utilizes PLGA as encapsulation matrix to prepare various CPNs with uniform morphology. Green et al. [41] used the similar method to synthesize CPNs capable of emitting visible spectrum of light. To accomplish this, the CPs was completely dissolved in DCM, 1,2-Diacyl-sn-glycero-3-phosphoethanolamine-N-[methoxy(polyethylene-glycol)-2000] (PEG_{2000}-PE) and 1,2-dipalmitoyl-sn-glycero-3-phosphocholine (DPPC) were added into the water, and then the CPNs encapsulated by PEG-lipid were formed by ultrasonic treatment. This method was simple, easy to operate, and the colloidal stability of the product was comparatively high.

Nanoprecipitation method

In the reprecipitation method, the CPs dissolved in a suitable organic solvent is rapidly injected into the water and subjected to ultrasonication. Then, the nanoparticles with uncertain colloidal stability are obtained after the removal of organic solvents (Fig. 2b). Nanoprecipitation is an extension of reprecipitation, in which the additional components called stabilizers (such as crude proteins) are typically added to the water-miscible solvent to obtain colloidal stable nanoparticles. The drastic change in the polarity of solvent leads to the aggregation of CPs to form corresponding nanoparticles and the size of obtained CPNs depends on the concentration of polymer used in the solution [17]. Landfester et al. [42] reported conjugated polymer dots (Pdots) with amphiphilic thiophene using a one-pot nanoprecipitation method. Pdots are small-sized spherical CPNs with high brightness and diameter comparable to that of quantum dots (< 20–30 nm). In this method, polythiophene derivatives and amphiphilic copolymer were co-precipitated into water under continuous ultrasonic conditions to obtain Pdots with small size (~ 16 nm in diameter), good dispersion and high fluorescence quantum yield ($\Phi = 0.15$). In 2017, Chen and co-workers [43] also employed nanoprecipitation method to obtain non-toxic Pdots with small particle size and high brightness. In the ordinary reprecipitation process, the polymer chain could easily be folded and collapse due to the hydrophobic interaction, thus, the further coupling of Pdots was promoted by adding a small amount of polystyrene-maleic anhydride (PSMA) to obtain stable nanoparticles. In the same year, Habuchi's group [44] used nanoprecipitation method to gain ultra-small Pdots (diameter = 3–4.5 nm) with excellent absorption cross-section and high fluorescence quantum

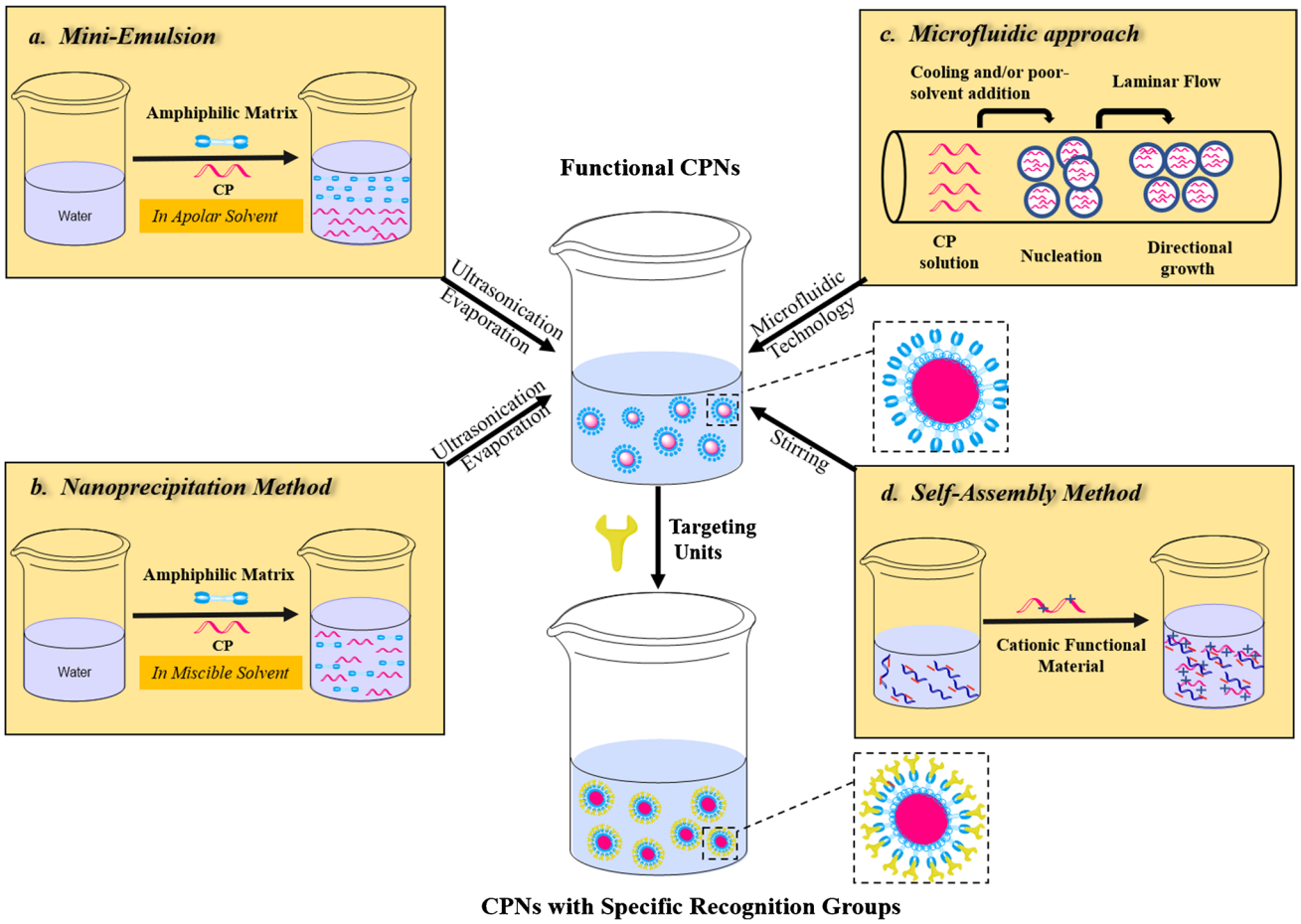

Fig. 2 Demonstration of frequently used methods for the preparation of CPNs. (**a**) Mini-Emulsion. (**b**) Nanoprecipitation. (**c**) Microfluidic approach. (**d**) Self-Assembly

yield (Φ = 0.16–0.20). Briefly, a very small amount of CP was dissolved in tetrahydrofuran (THF) to prepare the low concentrated polymer solution. After intense ultrasonic treatment at 277 or 343 K, the solution of CP was added to water, followed by evaporation of THF to obtain Pdots with excellent photostability. Thus, nanoprecipitation is a most common and useful method for obtaining CPNs.

Microfluidic approach

The microfluidic method has attracted great attention by the researchers, since it exhibits the capability of adjusting the size of nanoparticles by changing the flow rate of the polymer and the volume of poor solvent. This high-throughput method can control the morphology of the CPs by using the nanoscale volume of fluid in the microscale fluid channel, and can produce spherical or linear CPNs. The process of preparing CPNs by microfluidic system mainly includes the formation of nucleus and the crystal fiber. The polymer solution is cooled and nucleated under the condition of flow. After UV light irradiation, the degree of order and the planarization between the main chains of polymerization increased, and the CPs undergo aggregation with the decrease in the solubility, forming highly ordered crystal fibers (Fig. 2c) [45]. Moffitt's group [46] demonstrated the feasibility of the microfluidic system to assemble CPs into a fluid-variable micelle. In this study, the shear forces generated by the flowing environment inside the chip could control the nanostructures. On transferring the micellar dispersion from the reactor to the water environment, it could be collected along the treatment channel into the containing vials, because the vials contain deionized water that caused the nanoparticles to freeze dynamically. Reichmanis' group [47] prepared polythiophenyl based CPNs films using a microfluidic system and applied them in the fabrication of organic field-effect transistors (OFET) devices. Moffitt's research group [48] reported CPNs of different sizes and shapes on a chip in a two-phase microfluidic reactor at different flow rates. The microfluidic chip of this system was made up of polydimethylsiloxane (PDMS), and the size and internal structure of the polymer were adjustable by the shear force in the microchannel.

Self-assembly method

This is one of the recently emerging methods of preparing CPNs. It refers to the process in which the polymer molecules are spontaneously constructed into nanoparticles with special structure and shape under the action of electrostatic interaction, hydrogen bonding, van der Waals forces, and hydrophobic interaction (Fig. 2d). For example, the oppositely-charged CPs and co-assembled reagents are independently dissolved and dispersed in water [49]. After mixing in a strict proportion, the various forms of CPNs are obtained through high-speed centrifugation. Liu et al. [50] designed and prepared CPNs by electrostatic interactions between cationic pentathiophene and anticancer drug sodium chlorambucil. Hawker et al. [51] designed a controllable CPNs preparation scheme using a self-assembly method. In this study, the fixed geometric templates and adjustable interface interactions were combined to attain striped, ellipsoidal CPNs. Thus, using self-assembly approach, CPNs could be easily obtained through regulation of various types of interactions.

Soft template-based emulsion–dispersion polymerization

In emulsion polymerization process, ionic surfactants are typically used as soft-templates. In brief, an appropriate surfactant solubilizes the insoluble monomer followed by diffusion of initiator into the surfactant micelles to initiate polymerization. Then, the propagating chains of polymer are shaped by the micelle which ultimately yields highly spherical monodisperse particles with good stability in solution state (Fig. 3a). Weder and co-workers [52] utilizes the water-tolerance of the Sonogashira reaction in the preparation of PPE based micro- and nanoparticles. The cross-coupling reaction was realized inside the hydrophobic interior of anionic surfactant sodium dodecyl sulphate after proper dispersion of respective monomers, base, catalyst and solvent in aqueous media. 1,2,4-tribromobenzene was also added as co-monomer which assist in producing cross-linked polymer chains with good redispersibility in organic solvents. This method has been successfully employed for acquiring CP micro- and nanoparticles through polymerization of acetylene [53], pyrrole [54] and 3,4-ethylenedioxythiophene (EDOT) [55, 56], respectively.

Hard-template approach

While soft-template methods exhibit various features and remain versatile for preparing CPNs, the morphologies acquire through this method are fairly limited and shapes are much prone to deformation, since CPNs obtained using this approach exhibit structural stability only in solution state.

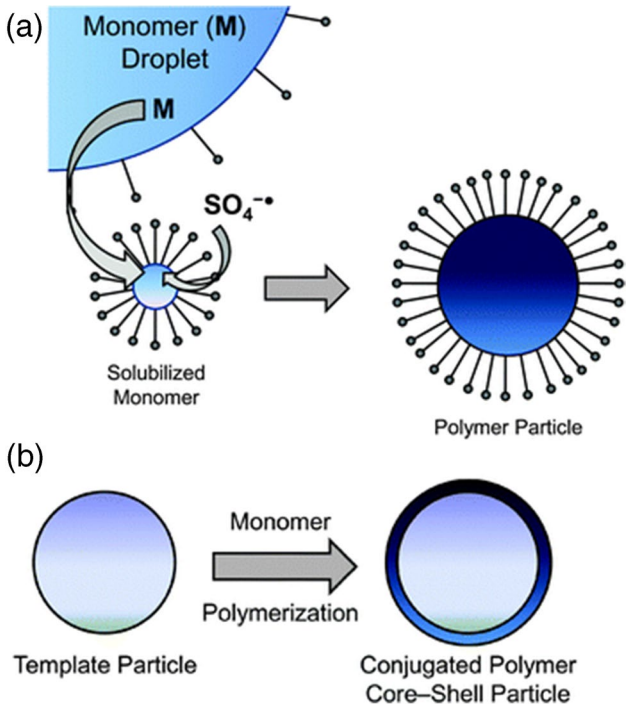

Fig. 3 (**a**) Soft template-based emulsion-dispersion polymerization method. Ionic surfactant solubilizes the monomer in aqueous media with hydrophobic tail followed by diffusion of water soluble initiator into the micelles to initiate polymerization. CPN is finally formed through replenishment of monomer within the micelle through diffusion from larger droplets. (**b**) Hard template based core–shell particles formation through polymerization onto the surface of silica or polystyrene templates. Reproduced with permission from reference [27]

The CPNs fabricated using hard-templates are much more reliable and shape persistence even in solid state. Two most common examples of this method include CP core–shell particles and silica nanocomposities. In core–shell structures, the shape of particle is controlled by silica or polystyrene core, whereas CP on shell facilitates desired optoelectronic properties (Fig. 3b). Earlier, CP core–shell particles has been obtained by coating polyaniline and polypyrrole films onto the surface of sterically stabilized polyurethane latexes which displayed excellent stability and good film forming ability [57, 58]. Later, Armes et al. demonstrated upgraded method to acquire a series of polyaniline [59], polypyrrole [60, 61], and PEDOT-coated [62] polystyrene latexes.

The amount of CP intact in core–shell particles is essentially low which remains as biggest disadvantage of the technique. To overcome this limitation, Wolf's research team [63, 64] developed another method for attaining CP micro- and nanocomposites by employing mesoporous silica sphere (MSS) as hard template. Nevertheless, this method also holds some vital features of the polystyrene and silica templates. Briefly, CP@MSS composites can be attained after intrusion of monomers inside the mesopores followed

by annealing and polymerization process. Interestingly, in CP@MSS composites, the CP is well-dispersed throughout the sphere and not merely on the surface of particle.

Thus, the overall loading capacity of CP in such composites can be amplified appropriately without affecting particle's colloidal stability, monodispersity and spherical geometry. Since its discovery, various types of CP@MSS materials have been successfully accomplished and studied employing PT, PEDOT and PPy composites [65] with mesopores ranged from 0 to 100%.

Biosensing applications of CPNs

The CPNs endowed with unique signal amplification property, high photostability, sensible fluorescence quantum yield and low toxicity represents one of the most promising candidates in the area of fluorometric detection. The CPNs can be easily employed for the detection of desired analytes employing variable signal transduction processes. Most common detection strategies include disruption of Förster resonance energy transfer (FRET), photo-induced electron transfer (PET), aggregation-induced FRET, charge transfer, perturbation of conjugation and aggregation-caused quenching (ACQ) mechanism. These processes typically require favorable interactions between the analytes and CPNs to be operative and bring change in signal. Based on these strategies, numerous probes based on CPNs have been reported in past for the detection and estimation of various biological molecules as discussed in the next section. Diverse research groups across the world including Bazan's, [35, 66], Swager's [8, 67], Wang's [68, 69], Liu's, [70, 71], Iyer's, [10, 72] etc. has contributed significantly in this direction. Some representative examples based on most common detection methods are discussed below.

Determination of cell-surface glycoprotein CD-44 via *disruption of FRET*

CD44 is a cell-surface glycoprotein associated with a variety of physiological processes, such as activation of white blood cells, invasion of cancer stem cells in tumors, and cell migration [73]. Meanwhile, it is also considered as a prognostic cancer biomarker [74]; therefore, it is vital to realize sensitive monitoring of CD44. Up to date, some cancer detection methods based on CD44 have been reported. The most common reverse transcription-polymerase chain reaction (RT-PCR) technique remain reliable and accurate but the operation processes remain complicated. For example, this method requires protein labeling, which makes the detection time-consuming and expensive. Therefore, the fluorescence technique with simplicity and high sensitivity has become an important detection method in biological analysis [75]. To accomplish fluorescence-based probes for CD44, the researchers typically labeled hyaluronan (HA) with organic fluorescent dyes because HA can bind efficiently and specifically to CD44. Huang and co-workers [76] designed another nanoprobe based on cationic CP poly{[9,9-bis(6′-(N,N,N-diethylmethylammonium)hexyl)-2,7-fluorenyleneethynylene]-alt-co-[2,5-bis(3′-(N,N,N-diethylmethylammonium)-1′-oxapropyl)-1,4-phenylene]} tetraiodide (PFEP) and fluoresceinamine-hyaluronan (FA-HA) complex for the sensitive, visual and facile recognition of CD44 and realizing CD44-mediated cancer cell imaging (Fig. 4). From zeta potential and SEM studies, it was proved that such spherical nanoparticle consists of hydrophobic dark core of PFEP and a hydrophilic shell of FA-HA [77–79]. In the presence of CD44, the FRET between PFEP and FA-HA was terminated which resulted in the recovery of blue emission color of PFEP, thus enabled the fluorometric estimation of CD44. The quantitative detection of CD44 was achieved by detecting the change in the ratio of the intensities of two fluorescence signals. The plot obtained from the concentration of CD44 from 0 to 1×10^{-7} g/mL against change in fluorescence intensity displayed a linear curve with correlation coefficient (R^2) of 0.9987. The limit of detection (LOD) was calculated to be 2.3×10^{-8} g/mL at a signal-to-noise ratio of 3. In contrast with reverse transcription-polymerase chain reaction (RT-PCR) that require protein labeling, this method only needs preparation of a solution containing PFEP/FA-HA nanoparticles followed by mixing the sample with the solution for the determination of fluorescence color under the naked eye using a portable UV lamp. After one year, the same research group [80] employed similar method to detect enzyme hyaluronidase (HAase) using nanoparticle fluorescent probe (PFEP/HA-Dox) based on CP PFEP and the hyaluronan-doxorubicin (HA-Dox) complex. Recently, Xiao and co-workers [81] also reported FRET disruption method for determination of enzyme glutathione S-transferase (GST) using glutathione (GSH)-modified fluorescent CPNs prepared by nanoprecipitation of CP poly[(9,9-dioctylfluorenyl-2,7-diyl)-co-(1,4-benzo-{2,1′-3}-thiadiazole)] (PFBT) with PSMA. In the subsequent year, same research group [82] demonstrated PFBT/PSMA nanoparticles for monitoring enzyme alkaline phosphatase (ALP) using FRET inhibition process. Zhang's research group [83] utilized FRET distraction process for determination of GSH at nanomolar level using CPNs prepared by co-precipitation of poly [3-{2,5-bis (2-ethyl-hexyloxy)}-phenyl]-vinyl]-9-ethylcarbazole] (PBEC) with PSMA.

Determination of enzyme tyrosinase via *PET*

Tyrosinase (TR) is an oxidase that controls the production of melanin and other pigments inside the body and also considered as a biomarker. Monitoring tyrosinase activity is

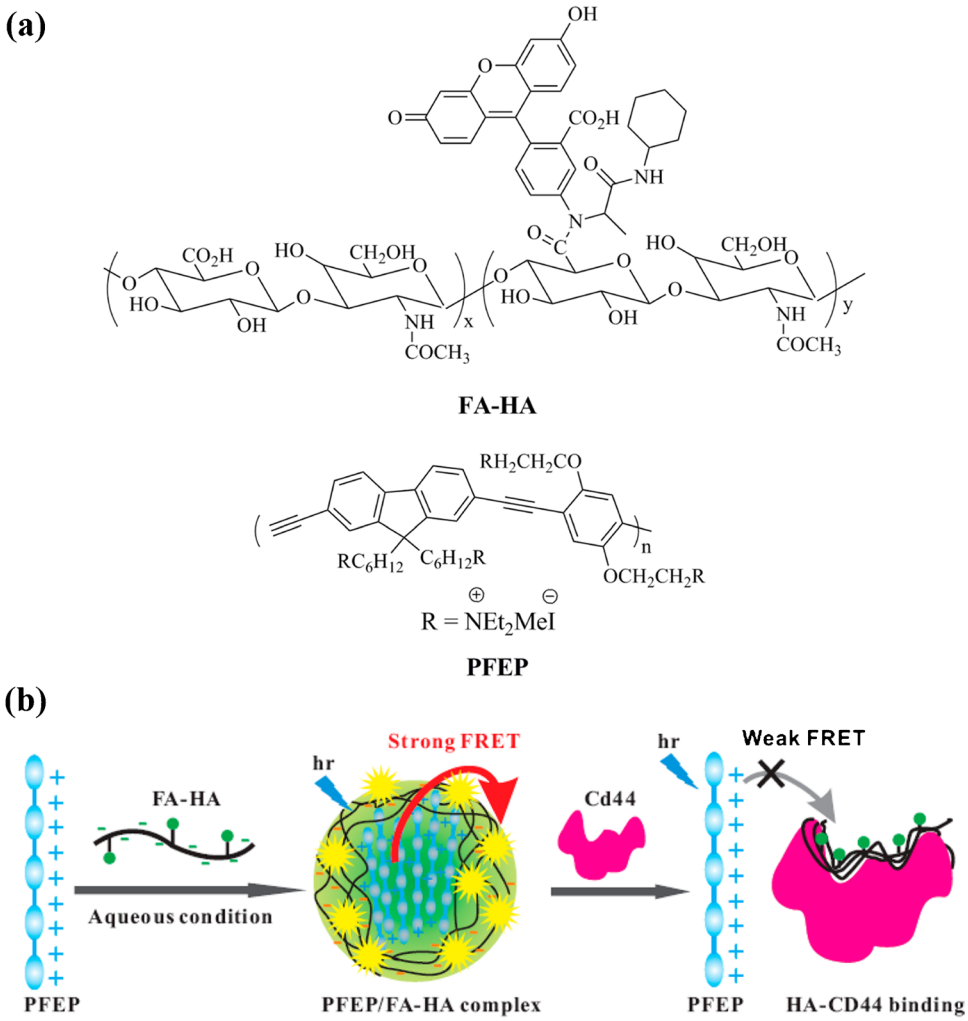

Fig. 4 Detection strategy for CD44. (**a**) Chemical structures of FA-HA and polymer PFEP. (**b**) PFEP interacts with FA-HA through electrostatic interactions and resulting nanoparticles formed facilitate the occurrence of FRET from PFEP to FA-HA. This triggers change in emission color of solution from blue to amplified green. The addition of CD44 which contains hyaluronan-binding domain resulted in breakdown of PFEP/FA-HA complex due to more favorable binding between FA-HA and CD44 and restores the blue fluorescence of PFEP via disruption of FRET. Reproduced with permission from reference [76]

extremely useful in the identification of Parkinson's disease and melanoma [84]. Feng's research group [85] designed an advanced sensing system based on functionalized Pdots with one-, two-photon excitation and dual-emission feature for high selective ratiometric detection and bioimaging of tyrosinase activity (Fig. 5). To accomplish this, poly(9,9-dioctylfluorenyl-2,7-diyl) (PFO) and poly[2-methoxy-5-(2-ethylhexoxy)-1,4-(1-cyanovinyl-1,4-phenyl)] (CN-PPV) were co-precipitated first and then further modified with L-tyrosine methyl ester (Tyr-OMe) by electrostatic interactions to acquire PFO/CN-PPV@Tyr-OMe Pdots as a probe for ratiometric monitoring of TR. The calibration curve obtained from changes in fluorescence intensity against variable concentration of TR displayed good linearity in the range 2.5 to 300 U/L with a R^2 value of 0.997. Additionally, the LOD value for TR was found to be as low as 1.1 U/L which meets the requirements for analysis of biological samples. Later on, Gao et al. [86] reported fabrication of Pdots via co-precipitation of PFBT with PSMA grafted with β-cyclodextrin (β-CD) for "turn-on" detection of GSH in living systems through GSH-induced inhibition of PET.

Determination of biogenic amines via *aggregation-induced FRET*

The aliphatic biogenic amines (BAs) are crucial molecules widely spread in the body and can be used as biomarkers to assess several human health disorders [87] including bacterial infections and cancer. Therefore, the development of a suitable method for rapid and sensitive detection of aliphatic BAs has become a research hotspot [88–90]. At present, the main methods for detecting aliphatic BAs include chromatography and capillary electrophoresis which are complicated, time-consuming and require expensive equipments [91–95]. In 2017, Xiaohui Wang and co-workers [96] designed a fluorescent "turn-on" sensor for efficient measurement of BAs based on carboxylated polyfluorene (PFTBTCOOH)/chitosan-graft-oleic acid (CS-graft-OA) fluorescent nanomicelles. Firstly, the CS-graft-OA was prepared via graft copolymerization of chitosan (CS) with oleic acid (OA) followed by the fabrication of CP nanomicelles through the self-assembly method (Fig. 6a, b).

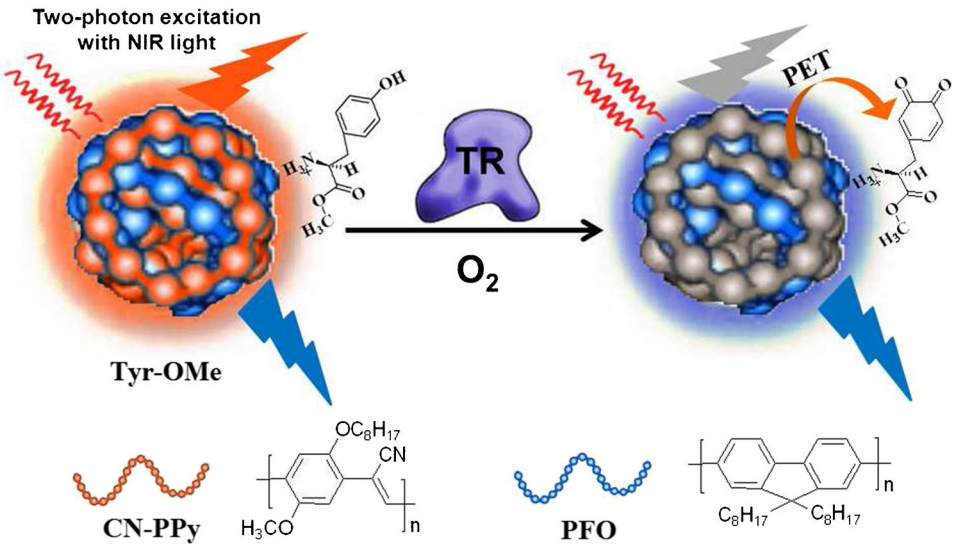

Fig. 5 The overall strategy for monitoring oxidative activity of tyrosinase (TR). CPs PFO and CN-PPV were first co-precipitated together to form blended Pdots followed by its functionalization with L-tyrosine methyl ester (Tyr-OME) via electrostatic interactions to attain a dual transmitter Pdots@Tyr-OMe nanoprobe. The nanoprobe displayed ratiometric change in emission color of solution from orange to blue through tyrosinase-induced catalytic oxidation of Tyr-OME via PET mechanism. Reproduced with permission from reference [85]

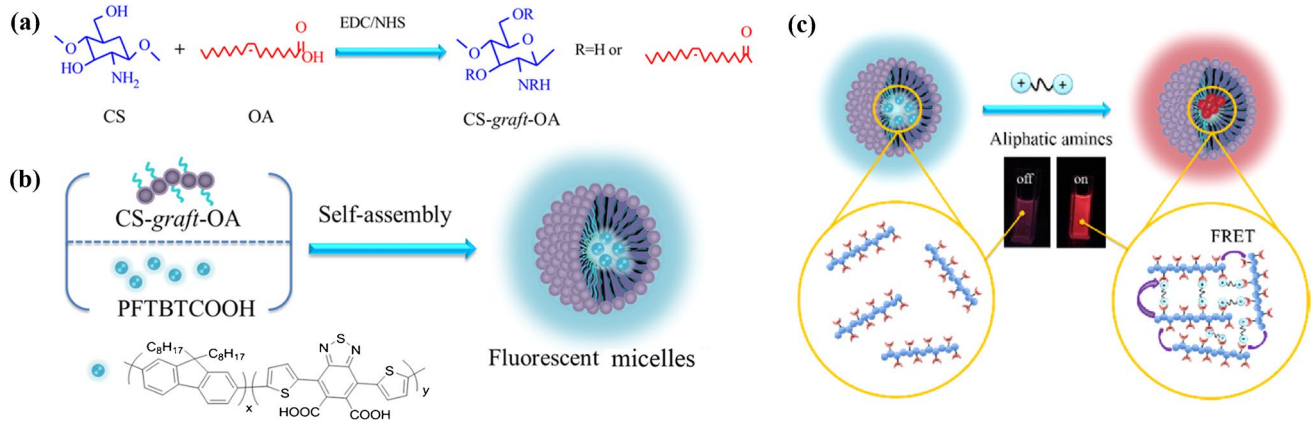

Fig. 6 Methodology adopted for the determination of aliphatic biogenic amines. (**a**) Preparation of CS-graft-OA. (**b**) Chemical structure of PFTBTCOOH and fabrication of fluorescent nanomicelles using self-assembly method. (**c**) PFTBTCOOH in nanomicelles interacts with aliphatic amines through electrostatic interactions and induces aggregation-enhanced FRET which ultimately triggers "turn-on" fluorescence response. Reproduced with permission from reference [96]

PFTBTCOOH is a polyfluorene derivative that displayed blue and red emission peaks of variable magnitude which varied on introducing aliphatic BAs (spermine, spermidine, putrescine and cadaverine) and promote ultra-sensitive and quantitative determination of aliphatic BA (Fig. 6c). Interestingly, the aromatic amines do not interfere during the detection of aliphatic BAs which confirms the high selectivity of this probe. Moreover, a linear curve with R^2 value of 0.983 was obtained between concentrations of cadaverine in range from 0–50 µM verses change in intensity, demonstrating the potential of nanomicelles for determination of cadaverine in aqueous solution. The LOD calculated for BAs was found to be 10 µM, indicating the reasonable sensitivity of probe. Employing mechanism of aggregation-induced FRET, Huang et al. [97] developed a ratiometric probe based on nanoparticles of newly prepared CP PF-DBT-PEG for determination of thiol. Li and colleagues [98] also reported determination of biomolecule adenosine triphosphate (ATP) through aggregation-induced FRET strategy using CPNs of emission color-tunable conjugated polymer PF-DBT-BIMEG.

Determination of neurotransmitter dopamine via *charge transfer*

Dopamine (DA) is the most abundant neurotransmitter in the brain and plays an important role in regulating the central nervous system [99–101]. Its abnormal level could be an indication of medical conditions [102] like Parkinson's disease, depression, etc. The electrochemical assay has become the favorable method for the detection of dopamine due to its convenience and promptness. However, due to

the similar oxidation potential between dopamine and many other substances, this method remains inefficient for achieving high selectivity. Moreover, the concentration of endogenous dopamine in the brain remains very low and highly susceptible to the interference by other biomolecules [103]. Shen's et al. [104] reported the fabrication of CPNs via self-assembly approach using CP PFPBA to detect dopamine in a solution, living cells as well as the brain of zebrafish larva (Fig. 7a). The surface of CPNs was also coated with PEG shell for reducing its immunogenic response and improving its distribution in vivo. The green color fluorescence of PFPBA nanoparticles was rationally quenched on addition of dopamine through the photo-induced charge transfer (Fig. 7b). A good linear relationship with R^2 value of 0.9907 can be observed between the concentrations of dopamine from 0.025 to 10 µM and change in emission intensity (Fig. 7b). The designed nanoprobe exhibits good selectivity over several other biomolecules with a very low LOD of 38.8 nM for dopamine. Moreover, the detection/imaging of neurotransmitter dopamine was also achieved in PC12 cells and brain of zebrafish larva which confirmed the applicability of nanosystem in the diagnosis of dopamine-related diseases.

Determination of hypochlorous acid via *perturbation of conjugation*

Like various ROS species, hypochlorous acid (HOCl) also played a vital role in many biological events and directly associated with the killing of variety of pathogens [105]. However, the condition of oxidative stress due to its excessive production in human body can cause inflammation-associated tissue injuries, such as lung injury, atherosclerosis, hepatic ischemia reperfusion injury, etc. Tang et al. reported [106] fabrication of blue emissive spherical CPNs (~200 nm) using CP poly [2,7-(9, 9'-dioctylfluorene)-co-alt-2,5-phenylamine] (PFAN) via reprecipitation method for the precise determination of HOCl (Fig. 8). The aniline groups along the backbone of PFAN are oxidized selectively by HOCl and deliver significant fluorescence quenching (>95%) response due to perturbation of conjugation. Moreover, the PFAN nanoparticle system demonstrates good

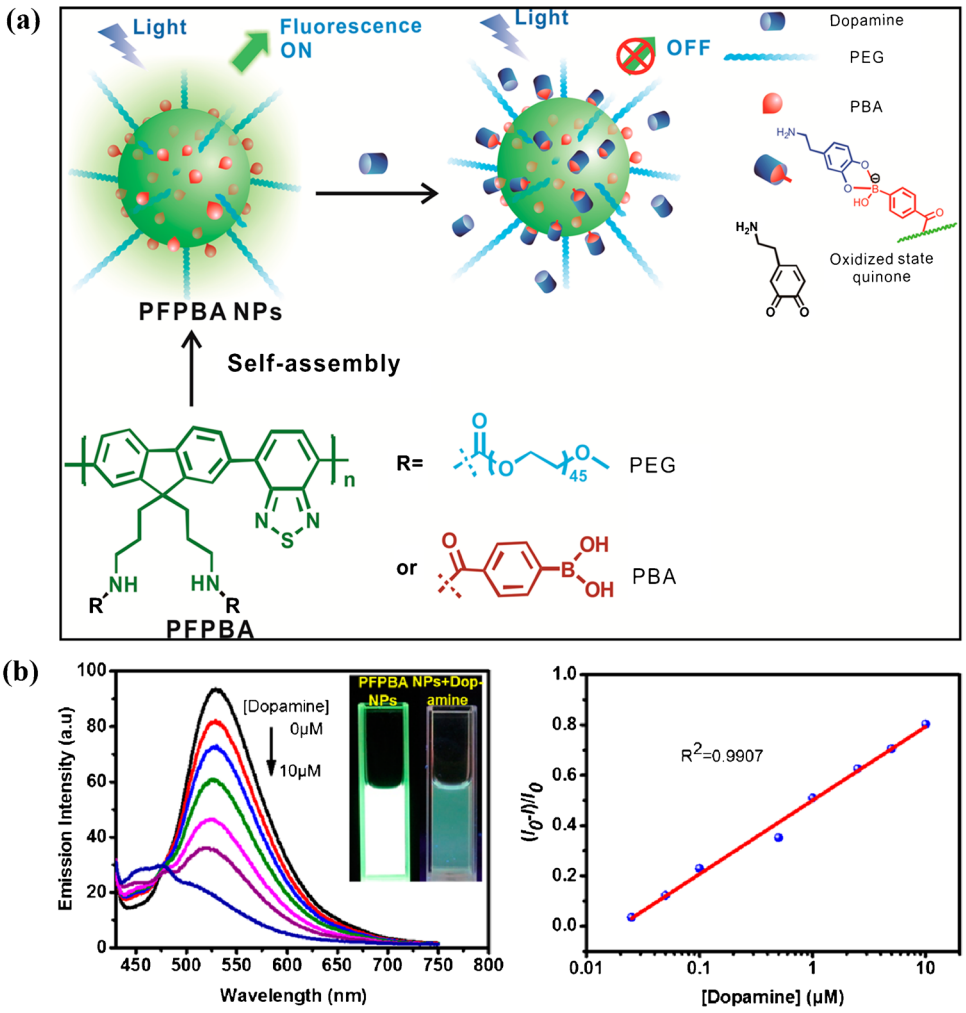

Fig. 7 (**a**) Sensing strategy for neurotransmitter dopamine using PFPBA-NPs. The self-assembly of PEG and phenylboronic acid (PBA) functionalized CP PFPBA led to formation of green emitting PFPBA NPs. The PBA groups tagged on the surface can bind selectively with dopamine molecules and converted into stable borate esters. An effective charge transfer between PFPBA NPs and dopamine or its oxidation product quinone ultimately causes efficient fluorescence quenching. (**b**) Change in fluorescence intensity of PFPBA NPs upon addition of dopamine and corresponding calibration plot showing good linearity. Reproduced with permission from reference [104]

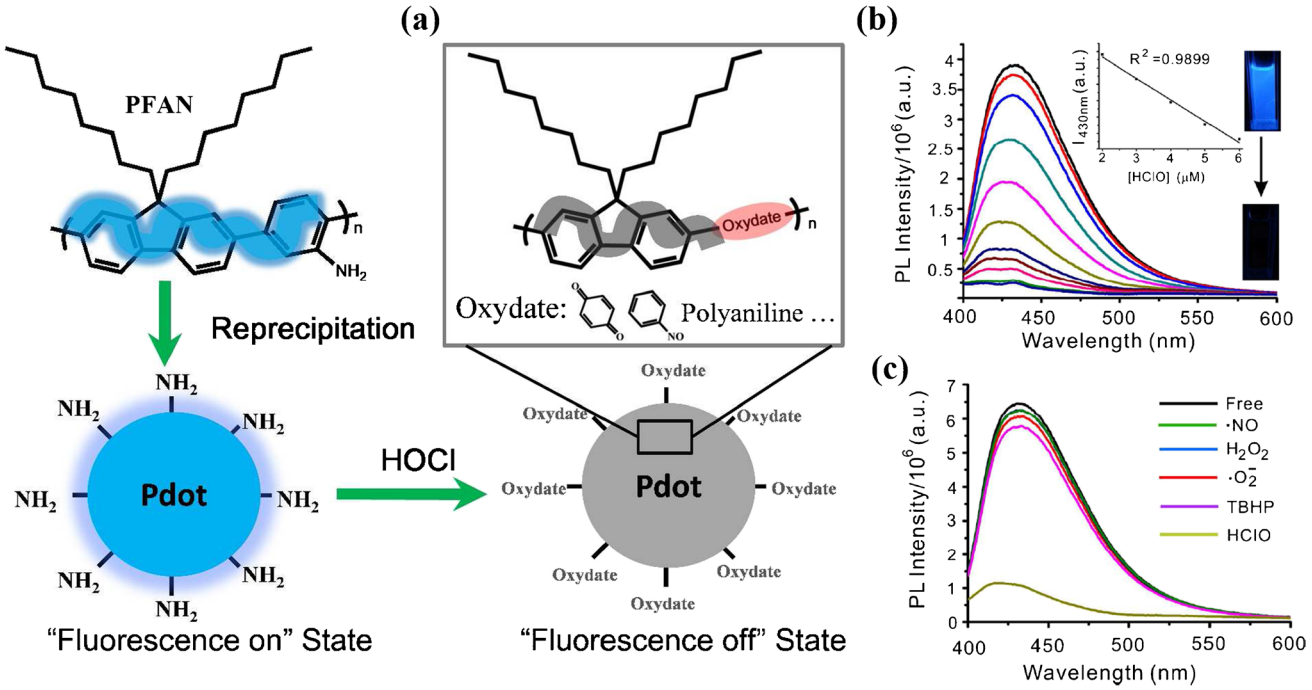

Fig. 8 (**a**) Fabrication of aniline based conjugated polyfluorene PFAN into blue emissive spherical PFAN NPs via reprecipitation method. Fluorescence quenching response of fabricated PFAN NPs with HOCl due to oxidation of aniline groups and subsequent perturbation of conjugation. (**b**) Change in fluorescence intensity of PFAN NPs (1 μM) at 430 nm with various concentration of OCl^- (0–15 μM) in water. Insets: The calibration curve demonstrate good linear relationship in the concentration range 2–6 μM with correlation coefficient (R^2) of 0.9899. Change in color of PFAN NPs dispersion in water before and after addition of OCl^-. (**c**) Change in fluorescence intensity of PFAN NPs with various competitive ROS species confirming selectivity of probe towards HOCl. Reproduced with permission from reference [106]

selectivity and reasonable LOD value of 0.5 μM for HOCl which is among the best reported value.

Fe (III) sensing based on aggregation-caused quenching (ACQ) mechanism

Iron is an essential element that performs multiple biological functions inside the human body. The abnormal level of Fe (III) ions can cause several diseases [107] like anaemia, Alzheimer's disease and Parkinson's syndrome, thus, the determination of Fe (III) ions is highly important for accurate monitoring of human health. To overcome the limitations in existing probes for Fe (III) ions, Xiaoju Wang and co-workers [108] reported fabrication of spherical CPNs (~75 nm) with high fluorescence quantum yield (Φ = 0.32) via simple reprecipitation process using newly designed CP PFP-PEG (Fig. 9a). The fabricated PFP-PEG NPs displayed good photostability, low cytotoxicity and utilized successfully for the determination of Fe (III) ions through aggregation-induced fluorescence quenching mechanism (Fig. 9b–d). Additionally, the LOD value of PFP-PEG NPs towards Fe (III) ions is found to be as low as 10^{-7} M which meets the requirements for analysis of biological samples. In subsequent years, Zhang and co-workers [109] also reported fabrication of CPNs by co-precipitation of CP poly[3-{2-[2,5-Bis-(2-ethyl-hexyloxy)-4-propenyl-phenyl]-vinyl}-9-butyl-6-methyl-9H-carbazole] (PBMC) with PSMA for detection of Fe (III) ions via ACQ mechanism and LOD as low as 0.63 nmol/L, respectively.

The above discussed papers related to the biosensing using CPNs and their nanohybrids are summarized in the Table 1.

Imaging using CPNs

Fluorescence imaging in vitro or in vivo using CPNs is highly preferred in the area of healthcare owing to their good biocompatibility, low cytotoxicity, remarkable photostability and excellent fluorescence brightness. In past, various CPNs have been utilized for specific and non-specific imaging [18, 27, 29, 32, 110, 111]. Specific imaging is usually performed using CPNs with some specific recognition groups and highly desired over non-specific imaging. For the purpose of diagnosis, various types of cancer cells have been utilized for targeted in vitro imaging using variable CPNs and their nanohybrids. For accomplishing efficient in vivo imaging, numerous far-red (FR)/near-infrared (NIR) emitting CPNs

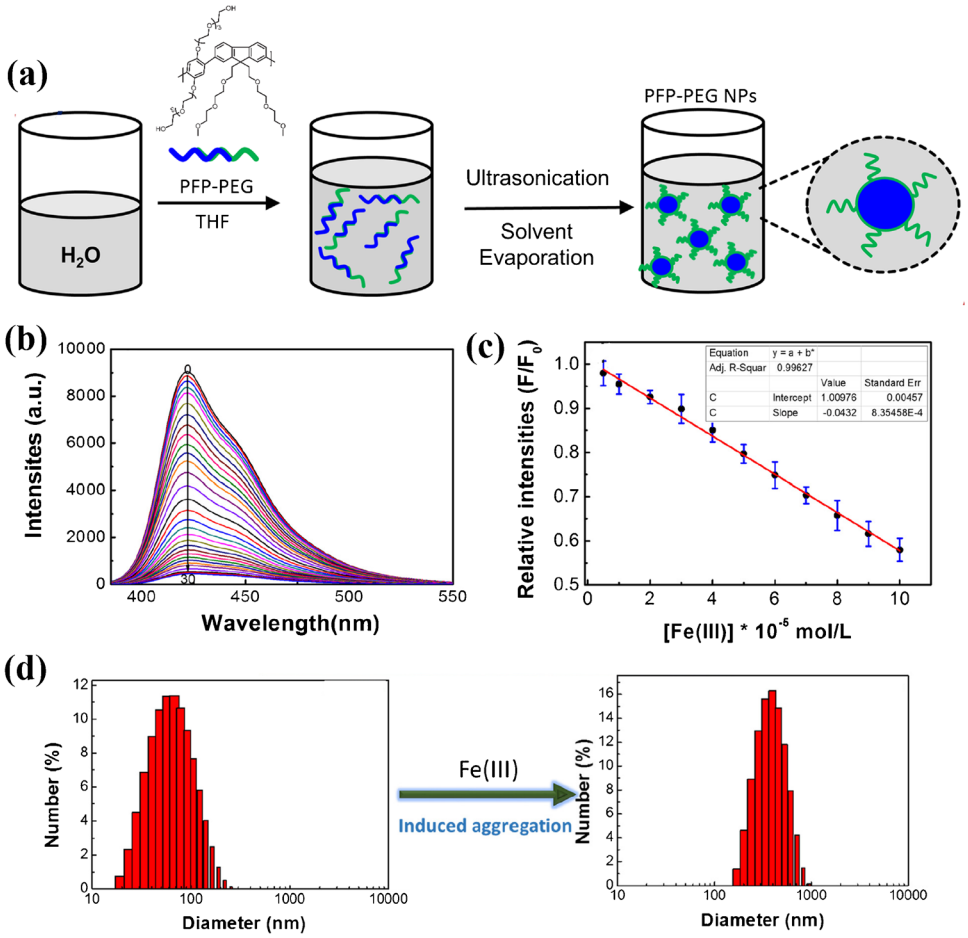

Fig. 9 (**a**) Transformation of CP PFP-PEG into PFP-PEG NPs using reprecipitation method. PEG groups on the surface of nanoparticles act as recognition sites for Fe (III) ions. (**b**) Changes in the emission spectra of PFP-PEG NPs ($\lambda_{ex} = 375$ nm) with continuous addition of Fe (III) ions. (**c**) Calibration curve obtained from the change in emission intensity against various concentration of Fe (III) demonstrate good linear relationship upto 10 µM concentration with R^2 value of 0.99627. (d) Dynamic light scattering (DLS) spectra depicting change in size of PFP-PEG NPs from 75 to 400 nm after addition of Fe(III) ions confirming the role of aggregation process in sensing. Reproduced with permission from reference [108]

and nanohybrids with minimal autofluorescence and better penetration have also been established [112–117]. Some of them are highlighted thoroughly in the following text.

In vitro *imaging*

The dual-color imaging probes exhibit advantages over single color probe in performing the precise analysis by minimizing the effect of autofluorescence. FRET technique [118, 119] plays an important role in realizing multicolor imaging and is highly beneficial for cell counting, clinical diagnosis, tumor detection and so on. As shown in Fig. 10a, Bazan's research group [120] designed and synthesized carboxyl functionalized CPNs by hydrophobic co-precipitation of blue (P1), green (P2), yellow (P3) and red (P4) emitting CPs with poly(styrene-co-maleic anhydride) (PSMA). The fabricated spherical CPNs displayed multicolor imaging characteristics using a single excitation wavelength (Fig. 10b). By varying the ratio of the four polymers, the emission could be adjusted [121, 122] by modulating the FRET. In addition, PSMA with carboxyl functional groups was further modified with primary antibody (anti-EpCAM) to obtain CPNs-antibody conjugates. CPNs-antibody conjugates were then employed successfully to specific multicolor imaging of the cancer cells facilitating the diagnosis (Fig. 10b). Moreover, the improved selectivity for imaging was observed using two CPNs labeled with different antibodies instead of a single-antibody recognition mode. Thus, the designed strategy not only facilitates targeted multicolor imaging of specific cancer cells but also avoids the use of multiple excitation sources.

Apart from nanoparticles, relatively small-sized conjugated polymer dots (Pdots) have also drawn widespread attention because of their fascinating optical features and non-toxicity [123]. In fact, Pdots have aroused [124–126] as favorable smaller sized nanomaterial compares to quantum dots (QDs) and upconversion nanoparticles (UCNPs) that are usually more toxic and less biocompatible. Though, it is difficult to functionalize Pdots with targeting species owing to their high hydrophobicity. The co-precipitation with amphiphilic molecules can smartly overcome this challenge as it makes the Pdots hydrophilic [127]. Jinyi Wang and co-workers [128] developed a folic acid (FA) and horseradish peroxidase (HRP)-bifunctionalized Pdots (FH-Pdots) for achieving on-site fluorescence imaging of cancer cells. To accomplish this, firstly, the strong amphiphilic Janus

Table 1 CPNs and their nanohybrids for biosensing applications

Conjugated Polymer	Matrix	Size	λ_{ex}	λ_{em}	Sensing Analyte	Sensing Mechanism	LOD Value	Linear Range and R^2 value	Ref
PFEP	PFEP/FA-HA	200–350 nm	405 nm	525 nm	CD44	Disruption of FRET	2.3×10^{-8} g/mL	Up to 10^{-7} g/mL, 0.9987	76
PFEP	PFEP/HA-Dox	30–50 nm	405 nm	445 nm	Hyaluronidase (HAse)	Disruption of FRET	0.075 U/mL	Up to 1.4 U/mL, 0.99002	80
PFBT	PFBT/PSMA/GSH	27 nm	473 nm	540 nm	Glutathione S-transferase (GST)	Disruption of FRET	1.03 ng/ml	0.01–6 μg/mL, 0.99	81
PFBT	PFBT/PSMA	17 nm	470 nm	540 nm	Alkaline phosphatase (ALP)	Disruption of FRET	0.01 μU/ml	0.031–12.4 μU/ml	82
PBEC	PBEC/PSMA	28.53 nm	430 nm	554 nm	Glutathione (GSH)	Disruption of FRET	20.4 nM	2–90 μM, 0.9962	83
PFO	PFO/CN-PPV	32 nm	380 nm	586 nm	Tyrosinase (TR)	Photo-induced electron transfer (PET)	1.1 U/L	2.5–300 U/L, 0.997	85
PFBT	PFBT/PSMA-β-CD	21.5 nm	450 nm	541 nm	Glutathione (GSH)	Inhibition of photo-induced electron transfer (PET)	2.7 nM	0.01–3 μM, 0.9912	86
PFTBTCOOH	PFTBTCOOH/CS-graft-OA	100–120 nm	380 nm	425 nm	Biogenic amines	Aggregation-induced FRET	10 μM	Up to 50 μM, 0.9833	96
PF-DBT-PEG	PF-DBT-PEG NPs	24 nm	380 nm	420 nm	Thiol	Aggregation-induced FRET	2.56 μg/mL	1–200 μg/mL, 0.996	97
PF-DBT-BIMEG	PF-DBT-BIMEG Pdots	100 nm	380 nm	420 nm	Adenosine triphosphate (ATP)	Aggregation-induced FRET	0.1 nM	30–70 μM, 0.9909	98
PFPBA	PFPBA Pots	120 nm	410 nm	529 nm	Dopamine	Charge transfer (CT)	38.8 nM	0.025–10 μM, 0.9907	104
PFAN	PFAN NPs	200 nm	373 nm	430 nm	Hypochlorous acid (HOCl)	Perturbation of conjugation	0.5 μM	2–6 μM, 0.9899	106
PFP-PEG	PFP-PEG NPs	75 nm	375 nm	422 nm	Fe (III)	Aggregation-caused quenching (ACQ)	10^{-7} mol/L	Up to 10^{-4} mol/L, 0.99627	108
PBMC	PBMC/PSMA	43.96 nm	420 nm	557 nm	Fe (III)	Aggregation-caused quenching (ACQ)	0.63 nmol/L	0.1–1 μmol/L, 0.9998	109

dendrimer and photosensitizer meta-tetra(hydroxyphenyl)-chlorin (m-THPC) were co-precipitated with the CP poly[2-methoxy-5-((2-ethylhexyl)oxy)-p-phenylenevinylene] (MEH-PPV) to prepare hydroxyl-terminated photosensitizer-doped Pdots (HO-Pdots). Then, the FA and HRP were covalently attached onto the Pdots to acquire FH-Pdots (Fig. 11a). In the designed nanosytem, the FA playes a role of tumor-targeting ligand and enhances the specificity of Pdots towards the cancer cells, whereas HRP helps in triggering the luminol-H_2O_2-HRP chemiluminescence system to generate light for exciting the probe. Both chemiluminescence resonance energy transfer (CRET) as well as FRET processes were employed simultaneously to realize the imaging of cancer cells without the need of any external light source. The red fluorescence of MEH-PPV based Pdots was mainly located around the cytoplasm and nucleus of cancer cells (Fig. 11b). The comparison of in vitro experiments on cancerous and non-cancerous cells proves the outstanding targeted fluorescence imaging capability of FH-Pdots. Interestingly, by co-cultivating FH-Pdots and cancer cells, the cell metabolic activity could be detected by the MTT method without adding any additional luminescent substrates. According to the fluorescence imaging studies, it was also observed that compared with ordinary organic dyes,

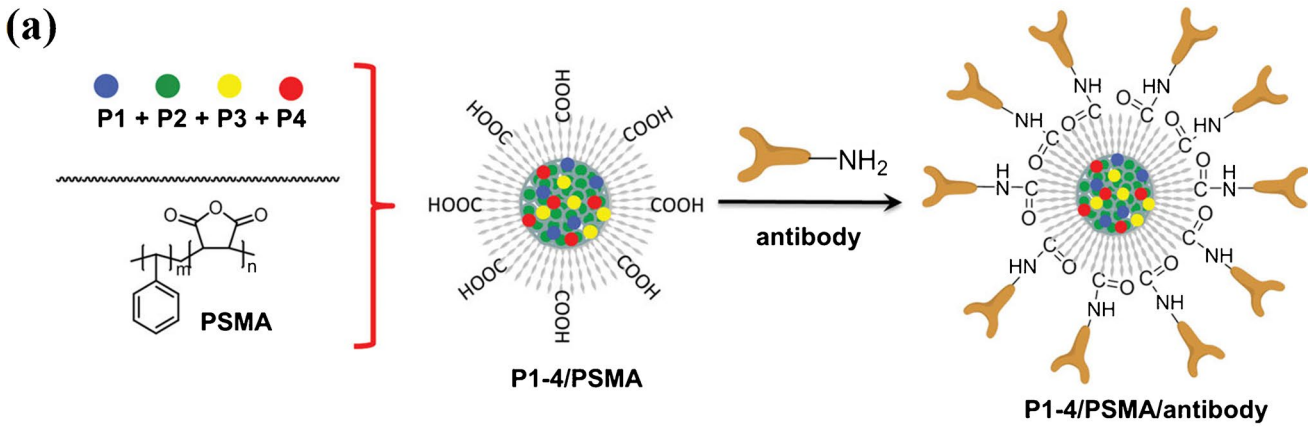

Fig. 10 (**a**) The preparation of multicolor CPNs (P1-4/PSMA) and their further modification with an antibody. (**b**) Multi-channel fluorescence images of MCF-7 cells using P1-4/PSMA/anti-EpCAM CPNs under different excitation wavelengths of 405, 488 and 559 nm, respectively. Reproduced with permission from reference [120]

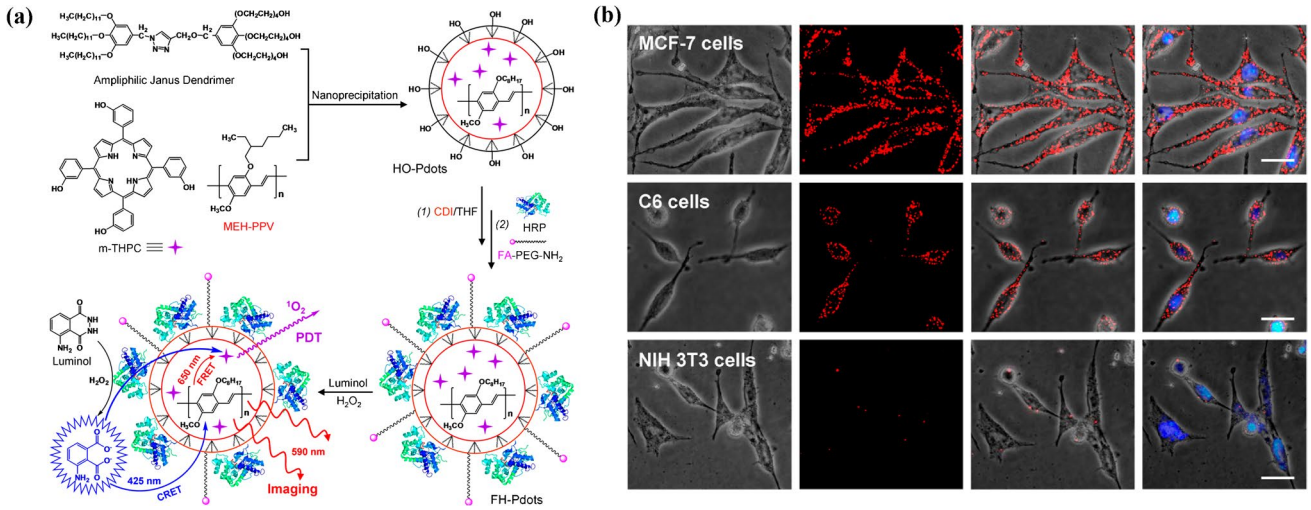

Fig. 11 (**a**) HO-Pdots were prepared first by co-precipitation of m-THPC, MEH-PPV and amphiphilic Janus dendrimer. HRP and FA were then covalently conjugated on HO-Pdots to obtain tumor-targeting FH-Pdots. (**b**) Fluorescence imaging of cancerous (MCF-7 and C6 cells) and non-cancerous (NIH 3T3 cells) cells after incubation with FH-Pdots for 6 h. The red fluorescence indicates the presence of FH-Pdots while blue emission corresponds to staining of nuclei by Hoechst 33,258. Reproduced with permission from reference [128]

FH-Pdots exhibit higher photostability and could achieve rapid and effective cell imaging in the environment of reactive oxygen species (ROS). Additionally, the presence of m-THPC facilitate targeted photodynamic killing of cancer cells.

Most of the tissues in the body have maximum optical transparency in the biological NIR window (700–1000 nm). Conventional fluorescent probes are usually excited by UV light or visible light, thus, prone to the decreased penetration depth due to the absorption and scattering of light by cell structures and tissues [129–131]. An effective method to overcome the barrier of penetration depth is to design a fluorescent probe [132] which can be excited by NIR wavelength laser. Some common organic dyes has been reported for NIR fluorescent labeling but challenges like low brightness, high cytotoxicity [133, 134] greatly affects their performance. Tian and co-workers [135] designed a novel hybrid nanoprobe composed of CP poly[(9,9-di-n-octylfluorene-2,7-diyl)-alt-co-(2,5-bis(4-(N,N-(diphenylmino)styryl) benzene)-1,4-diyl)] (P-F8-DPSB) (as the energy donor) and fluorescent dye DPA-PR-PDI (as the energy acceptor) with both excitation and emission in the NIR region based on the FRET mechanism (Fig. 12). The results indicated that the fluorescent probe displayed excellent penetrating ability in the NIR region with both excitation and emission light, which determines its excellent performance in the deep tissue imaging. In addition, the nanohybrid probe demonstrates the ability to selectively identify cancer cells due to the grafting of FA receptors on the probe that can bind specifically to cancer cells overexpressed by FA receptors. Under the wavelength of NIR laser light (800 nm), a clear fluorescence image of nanoparticles could be observed even when the simulated tissue thickness was as high as 1200 µm, which verifies the practicability of this probe in deep tissue imaging.

The issue of self-quenching in the conjugated materials through π-π stacking after their conversion into

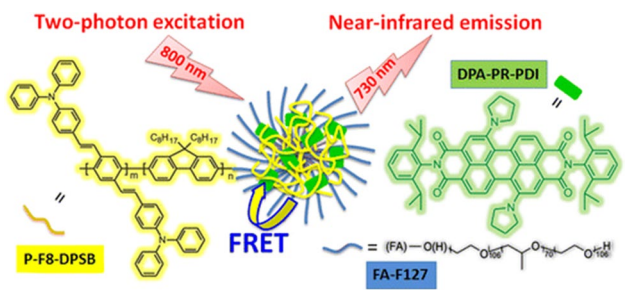

Fig. 12 The co-precipitation of CP P-F8-DPSB, DPA-PR-PDI and FA-F127 resulted in the formation hybrid CPNs which showed NIR emission at 730 nm due to combination of two-photon absorption based excitation under 800 nm pulse laser and efficient intermolecular FRET. Reproduced with permission from reference [135]

corresponding nanoparticles or dots critically affects their fluorescence efficiency especially of NIR probes that exhibit extensively conjugation. To attain high efficient NIR imaging probe, Chan and co-workers [136] developed an advanced imaging platform by systematic doping of common NIR dyes into CP poly[(9,9-dioctylfluorene)-co-2,1,3-benzothiadiazole-co-4,7-di(thiophen-2-yl)-2,1,3-benzothiadiazole] (PFBTDBT) to form a Pdot matrix via coprecipitation and then forming a layer of carboxyl-terminated polydiacetylene (PDA) as shown in Fig. 13. The polymer material in the matrix acted as light harvesting material and boosts the NIR efficiency of nanoprobe via intermolecular FRET. The carboxyl groups on PDAs could be further functionalized to target specific cells. To demonstrate the applicability of this newly designed system in cancer diagnosis, the PDA-coated Pdot matrix were coupled with streptavidin (SA) and used for targeted cell imaging of breast cancer cells (MCF-7) through antigen–antibody interactions.

The real-time monitoring of oxygen concentration is conducive for accurate diagnosis of retinal diseases, brain abnormalities and cancer [137]. Studies have proved that the probe based on the triplet excited state phosphorescent metal complex can achieve high resolution imaging of O_2, which is attributed to the existence of a triple ground state and triple excited state energy transfer process between O_2 and the metal complex [138, 139]. At present, the phosphorescent metal complexes probes are usually based on Pt (II), Ru(II), Pd(II) and Ir(III) complexes with long-lived triple excited states [140]. Since, these probes adopt a single phosphorescent emission mode; the detection signal could be easily affected by the external environment and liable for erroneous analysis. Huang's research team [141] successfully designed and fabricate fluorescent/phosphorescent dual-emissive Pdots (FP-Pdots) using self-assembly method of CP P2 and phosphorescent platinum (II) porphyrin for proficient imaging of hypoxia in human liver carcinoma cells (HepG2) through a FRET technique (Fig. 14a). The energy donor (fluorene) and the energy acceptor (platinum(II) porphyrin) units act as the O_2 insensitive and O_2 sensitive fluorophore, respectively. Thus, the variable change in the donor–acceptor fluorescence intensities was observed with different content of O_2 promoting the ratiometric monitoring of hypoxia in living cells through the FRET strategy. The probe's imaging technique for O_2 in living cells was performed via two methods, including photoluminescence lifetime imaging microscopy (PLIM) and time-gated luminescence imaging (TGLI). FP-Pdots and HepG2 cells were incubated with different oxygen concentrations and the average emission lifetime was increased from 17 to 95 ns when the O_2 concentration was decreased from 21 to 2.5%. (Fig. 14b). Such investigations confirm the applicability of designed nanoprobe for the determination of hypoxic conditions in living samples.

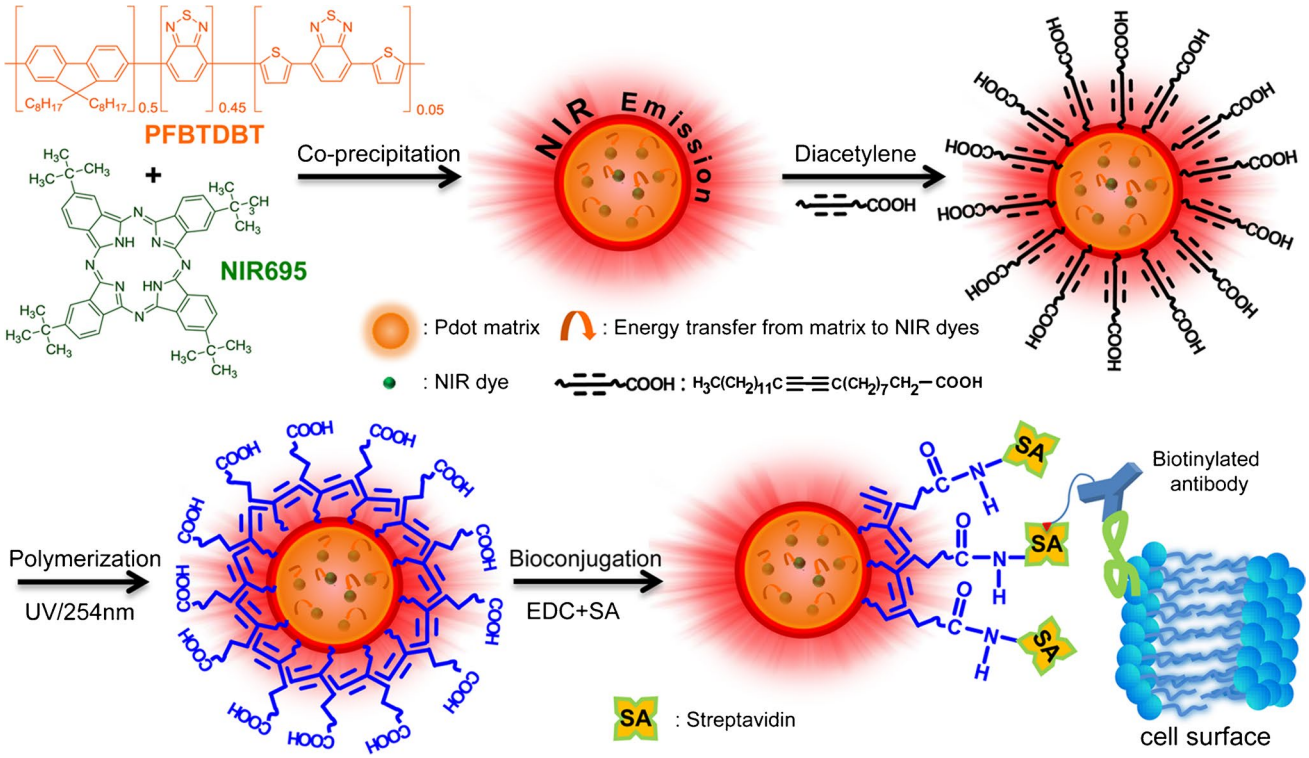

Fig. 13 FRET mediated NIR emitting Pdot matrix was prepared first by co-precipitation of PF-BT-DBT with NIR695. A layer of carboxyl-terminated polydiacetylene was then formed on the outer surface followed by functionalization with streptavidin for target-specific cell imaging through favorable antigen–antibody interactions. Reproduced with permission from reference [136]

Among various types of cancer, the number of cases related to triple negative breast cancer (TNBC) has been rising constantly and become the main cause of cancer-related deaths in women due to its ease of metastasis and high recurrence rate [142, 143]. The negligible or very low expression [144, 145] of human epidermal growth factor receptor-2, progesterone receptor and estrogen receptor in TNBC is responsible for its poor diagnosis. One possible solution to this issue could be the designing probe with targeting ability for integrins which are transmembrane receptors. In 2018, Xu's research group [146] designed and fabricated a fluorescent image-guided platform based on CPNs named as cRGD-MEH-PPV NPs for diagnosis as well as photodynamic therapy of TNBC (Fig. 15). Firstly, CP MEH-PPV as a photosensitizer was mixed with amphiphilic polymer 1,2-distearoyl-*sn*-glycero-3-phosphoethanolamine-N-[maleimide(polyethylene glycol)] (DSPE-PEG-MAL) in THF to obtain MEH-PPV NPs. Then, multiple units of cyclic arginine-glycine-aspartic acid (cRGD) polypeptide was coupled on the surface of the nanoparticle as a targeting group to obtain cRGD-MEH-PPV-NPs (Fig. 15a). The fluorescence intensity of cRGD-MEH-PPV-NPs only decreased by 30% after 30 days of incubation in the cell culture medium, which indicates the good photostability and the feasibility of probe for clinical diagnosis. To demonstrate the targeting imaging ability of fabricated nanoparticles, the nanoprobe was incubated with integrin-overexpressed MDA-MB-231 cells as well as two other cancers cells viz. MCF7 and NIH3T3 as control. The results indicated that there was obvious red fluorescence in the cytoplasm of MDA-MB-231 cells (Fig. 15b) and the fluorescence intensity of MDA-MB-231 cells was 30 times higher than that of other two cells, confirming the targeted imaging ability of cRGD-MEH-PPV nanoparticles and promising potential in the diagnosis of triple negative breast cancer.

In vivo *imaging*

After numerous in vitro imaging applications of CPNs, scientists further explored the role of CPNs in ex/in vivo imaging to gain vital information about various biological processes inside the body [147]. For e.g., monitoring ROS level inside the living system is crucial for diagnosis of diseases such as diabetes and cancer [148, 149]. Among numerous ROS radicals, superoxide anion radical ($O_2^{\bullet -}$) acts as a sink for several others radicals produced intracellularly. The traditional method of detecting $O_2^{\bullet -}$ is based on photon emission. However, due to the existence of external light excitation, this method remains vulnerable to the background fluorescence interference and light induced damage. Fortunately, the chemiluminescence technology that does not require the use of external light excitation source could

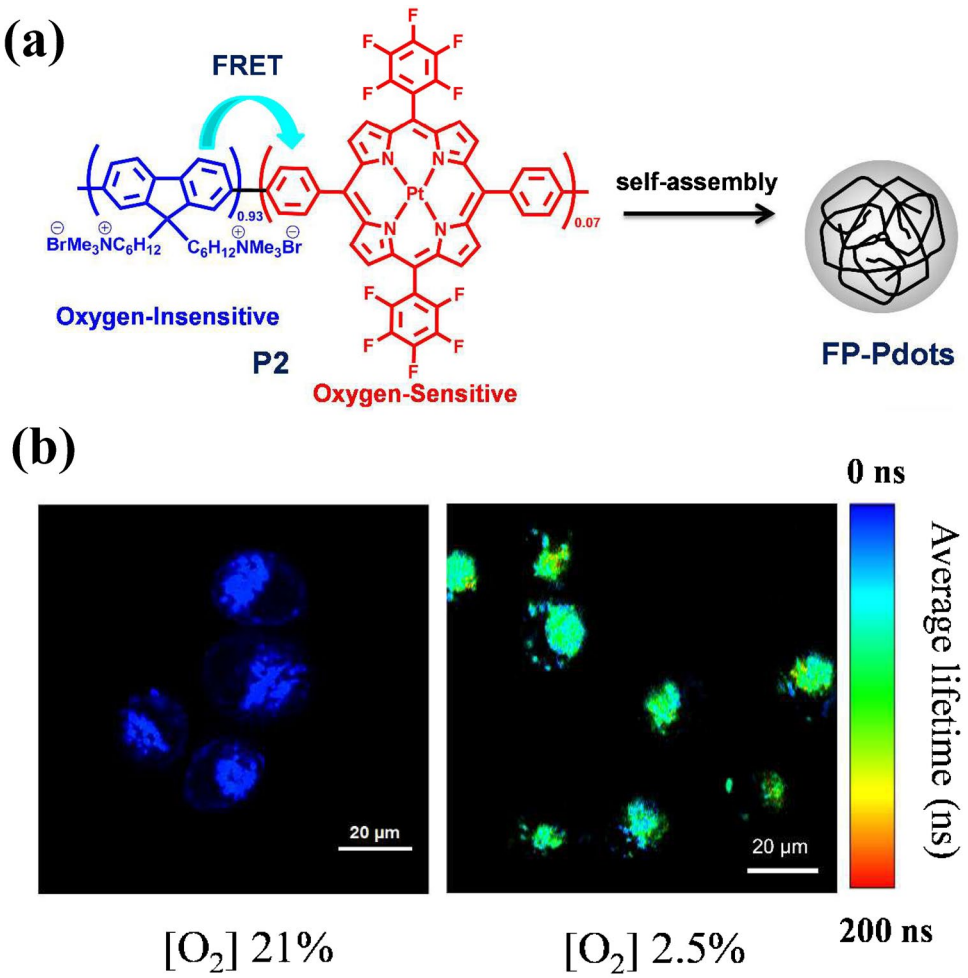

Fig. 14 (**a**) Chemical structure of fluorescent/phosphorescent CP P2 and fabrication of dual-emissive FP-Pdots. (b) Photoluminescence lifetime images observed for HepG2 cells incubated with FP-Pdots for 2 h at 21% and 2.5% O_2 concentrations. Reproduced from Ref. [141] with permission from the Royal Society of Chemistry

circumvent the above problems but exhibit the disadvantages of low emission intensity and short emission wavelength. Therefore, the CP with the phenomenon of CRET would be an attractive imaging probe for detecting endogenous $O_2^{\bullet-}$ because of its strong emission intensity and ability to maintain a long luminous time. Tang's research group [150] developed a nanoprobe using CP PCLA-$O_2^{\bullet-}$ via nanoprecipitation method and utilized it for in-vivo imaging of native $O_2^{\bullet-}$ through CRET process without the need of any external light excitation (Fig. 16). PCLA-$O_2^{\bullet-}$ consist of (1) imidazopyrazinone (CLA) moiety which acted both as energy donor unit and structural recognition unit for $O_2^{\bullet-}$ and (2) a polyfluorene backbone which acted as an energy receptor and also as a signal amplification matrix [151] (Fig. 16a). $O_2^{\bullet-}$ could activate CLA to produce chemiluminescence which facilitate proficient CRET with polymer backbone (due to efficient spectral overlap between chemiluminescence of CLA and absorption of polymer backbone) to ultimately generate luminescence of relatively higher magnitude and prolonged time for effective in vivo imaging of $O_2^{\bullet-}$ in mice (Fig. 16b). Recently, Ibarra's research team [152] developed a CP based nanoprobe consist of CP PFBT, polystyrene grafted with ethylene oxide functionalized with carboxyl groups (PS-PEG-COOH) and iron oxide nanoparticles (IONPs) for magnetic resonance and fluorescent imaging of brain tumors.

The background autofluorescence during imaging is the most common problem in bioimaging. To address this issue, materials with persistent luminescence have become the first choice for in vivo imaging studies because of their longer luminescence lifetime. Rao and co-workers [153] developed an advanced imaging platform based on CPNs with the exclusive feature of persistent luminescence close to 1 h. The nanoprecipitation of CP MEH-PPV with PS-PEG-COOH led to the formation of biocompatible and surface-functionalized nanoparticles denoted as NP (Fig. 17a). Moreover, the NIR emitting dye NIR775 was also encapsulated to attain nanoparticles with long-lasting NIR emission. The fluorescence energy of MEH-PPV molecules was transferred to the NIR775 dye through the FRET mechanism, resulting in a significant increment in the intensity of NIR emission peak (Fig. 17b, c).

Consequently, after subcutaneous injection of hybrid nanoparticles in mice, the persistent emission was applied for in vivo imaging which indicates the great potential of

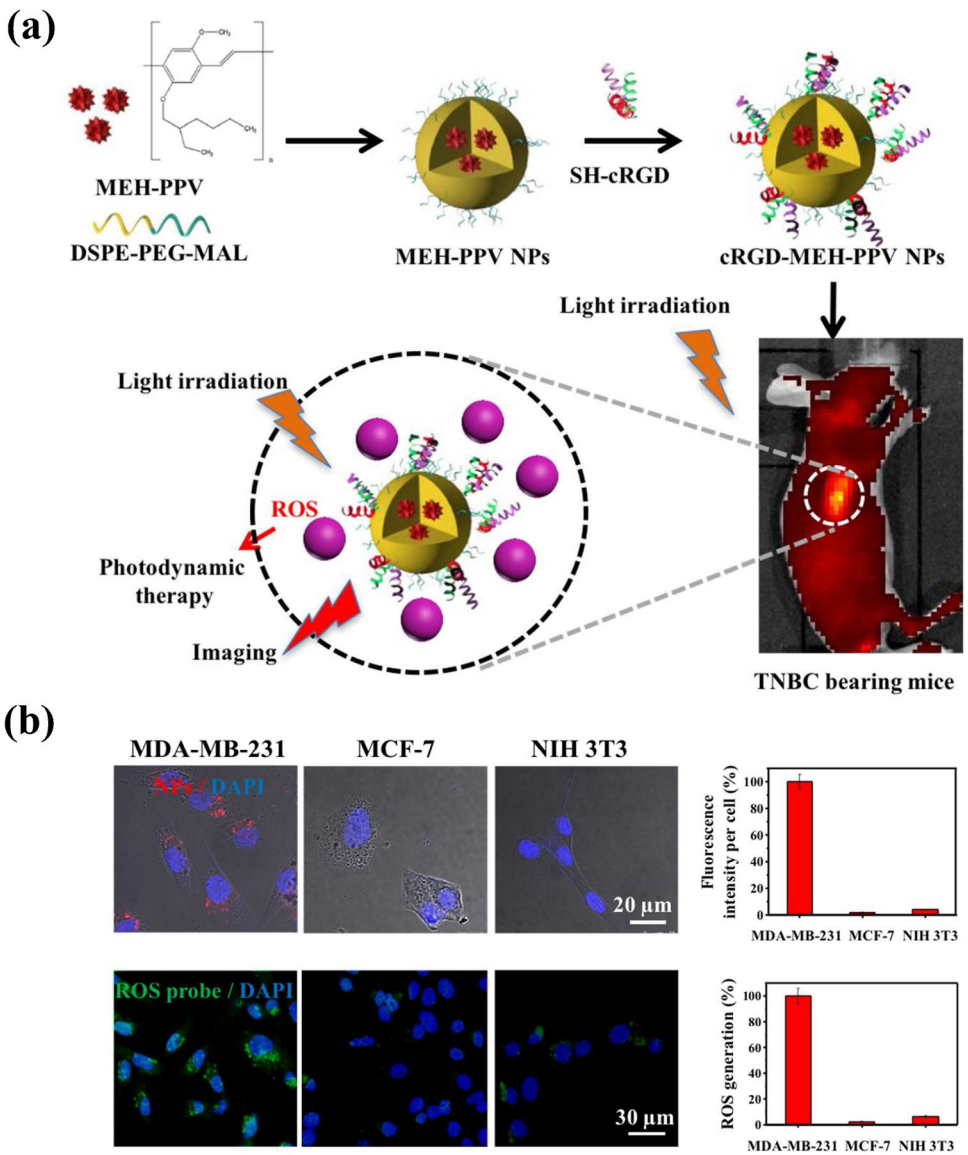

Fig. 15 (**a**) MEH-PPV NPs were prepared first through co-precipitation of MEH-PPV with DSPE-PEG$_{2000}$-MAL. cRGD-MEH-PPV NPs were then obtained by conjugation of MEH-PPV NPs with the target moiety (cRGD) that exhibit high affinity for integrin-over-expressed triple negative breast cancer cells. cRGD-MEH-PPV NPs can also release ROS to induce photodynamic therapy under light irradiation. (**b**) Targeted imaging, mean fluorescence intensity and ROS generation capability inside MDA-MB-231, MCF-7, and NIH 3T3 cells using cRGD-MEH-PPV NPs. The red emission indicates the presence of cRGD-MEH-PPV NPs, green color confirms the intracellular ROS and blue emission shows nuclei staining by 4',6-diamidino-2-phenylindole (DAPI). Reproduced with permission from reference [146]

the continuous luminescent nanoparticles in the field of in vivo tracking (Fig. 17d). Recently, a new type of NIR light emitting CPNs were fabricated [154] by sandwiching CP poly((9,9-dioctylfluorene-2,7-diyl)-alt-(4,7-di(thiophene-2-yl)-2,1,3-benzothiadiazole)-5′,5″-diyl) (PFTBT) in between the core and shell of crystalline silica for in vivo tracking of human umbilical cord mesenchymal stem cells in a mouse model with severe liver injury. Moreover, in vivo NIR-II fluorescence imaging of tumor is also reported [155] using newly developed CPNs prepared by nanoprecipitation of CP TTQ-2TC (bearing triazole[4,5-g]-quinoxaline (TTQ) and long alkyl side chains modified bithiophene (2TC)) with PS-PEG.

In addition to the widely studied fluorescence imaging technology [147], photoacoustic imaging (PAI) also a hold promising future in the area of theranostics because of its high spatial resolution and deeper tissue penetration ability [156, 157]. Current photoacoustic (PA) contrast agents include organic nanoparticles, gold nanorods (GNRs), porous materials, single-walled carbon nanotubes (SWCNTs), etc., among which CPNs display the highest PA signal output and good stability. The same research group [158] also designed a highly efficient, sensitive, and stable nanoplatform based on NIR light absorbing CPNs to achieve low-damage PA imaging of living organisms. In brief, two NIR light absorbing CPs SP1 and SP2 were nanoprecipitated separately in the presence of 1,2-dipalmitoyl-sn-glycero-3-phosphocholine (DPPC) to acquire corresponding water dispersible nanoparticles as SPN1 and SPN2 (Fig. 18a, b). The matrigel-containing solutions of these nanoparticles were injected subcutaneously into the dorsal area of mice for PA imaging (Fig. 18c). The PA signal obtained using

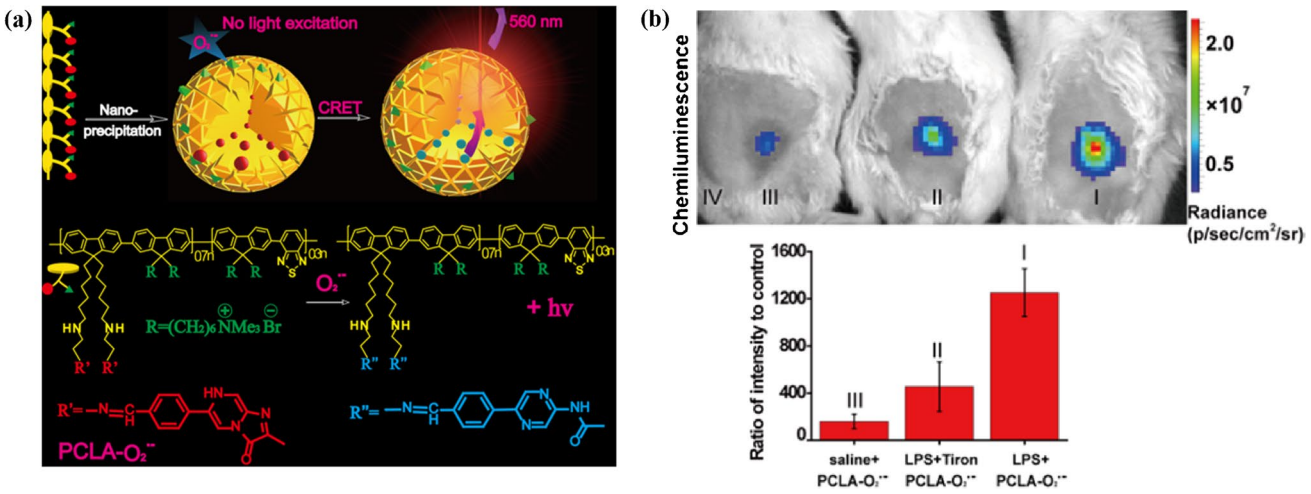

Fig. 16 (**a**) Preparation of PCLA-$O_2^{\bullet-}$ nanoparticles using cationic polyfluorene derivative by nanoprecipitation method and mechanism of $O_2^{\bullet-}$ detection. $O_2^{\bullet-}$ triggered the CLA groups and chemiluminescence produced (λ_{em} = 490 nm) is directly transferred to polymer backbone via CRET to finally emit an amplified light (λ_{em} = 560 nm) without requiring any external light excitation. (**b**) Chemiluminescence imaging of endogenous $O_2^{\bullet-}$ in the lipopolysaccharide (LPS) treated mice (n = 4) and ratio of chemiluminescence emission intensities to control at 0.5 min. (I) LPS + PCLA-$O_2^{\bullet-}$, (II) LPS + Tiron + PCLA-$O_2^{\bullet-}$, (III) saline + PCLA-$O_2^{\bullet-}$ and (IV) the control: saline. PCLA-$O_2^{\bullet-}$ showed brighter chemiluminescence in LPS-treated mice because of higher $O_2^{\bullet-}$ produced by inflammation. Reproduced with permission from reference [150]

these nanomaterials was ~ 5.8 and ~ 4 times higher than GNRs and SWNTs, respectively which demonstrates the superior performance of fabricated nanoprobes for in vivo PA imaging. Recently, Yuan and co-workers [159] reported protein modified NIR light absorbing CPNs by incorporation of bovine serum albumin (BSA) into CP poly((E)-3-(5-([8,8′-biindeno[2,1-b]thiophenylidene]-2-yl)thiophen-2-yl)-alt-2,5-bis(2-octyldodecyl)-6-(thiophen-2-yl)-pyrrolo[3,4-c]pyrrole-1,4(2H,5H)dione) (PBTP-DPP) for in vivo photoacoustic and fluorescence imaging of tumor.

The above discussed papers related to imaging applications using CPNs are summarized in the Table 2.

Theranostic applications of CPNs

Besides sensing and imaging, CPNs also showed encouraging results in the diagnosis and treatment of variety of health disorders like cancer, microbial infections, cardiac diseases and so on. Many CPNs and nanohybrids have been positively utilized as photosensitizer (for photodynamic therapy), photothermal agent (for photothermal therapy) and an efficient carrier of drug (for drug delivery). The distinct features of such type of CPNs are discussed below by taking some representative examples with emphasis on cancer as a model disease.

Photodynamic therapy (PDT)

Photodynamic therapy (PDT) is an efficient and non-invasive method of light-mediated treatment of the diseases using the materials termed as photosensitizers [160]. A photosensitizer molecule is stimulated by administering the light of a certain wavelength to create ROS primarily in the form of singlet oxygen ($^1O_2$) from the molecular oxygen ($^3O_2$). When a fluorophore is exposed to a particular light source, it creates a singlet excited state (S_1), which is then converted into a triplet excited state (T_1) by a non-radiative mechanism known as intersystem crossing (ISC) [161]. Transferring energy from T_1 sensitizes the production of $^1O_2$ from the ground-state $^3O_2$ as shown in Fig. 19. Such ROS is highly prone to kill tumor cells or microorganisms through various biological pathways [162]. Several photosensitizer conjugates or photosensitizer-loaded nanoparticles, such as polymeric micelles, gold nanoparticles, upconversion conjugated nanoparticles (UCNPs), carbon dots, and mesoporous silica nanoparticles, have been used in the image-guided therapy of cancer with enhanced PDT efficacy [163–173]. In contrast to small molecule photosensitizer, CP photosensitizer are more efficient in generating ROS owing to their unique light-harvesting properties and presence of many energy levels in each energy band (Fig. 19b).

During the transformation of triplet oxygen into singlet oxygen through PDT process, the molecular oxygen level inside the cells tends to decrease and facilitate hypoxic condition. Thus, the combination of a PDT system with a hypoxia-responsive drug delivery could be auspicious for achieving improved antitumor therapy. To realize this, Gu and co-workers [174] developed an innovative CP-based nanocarrier (DOX/CP-NI) capable of fluorescence imaging, producing light-activated ROS in addition to

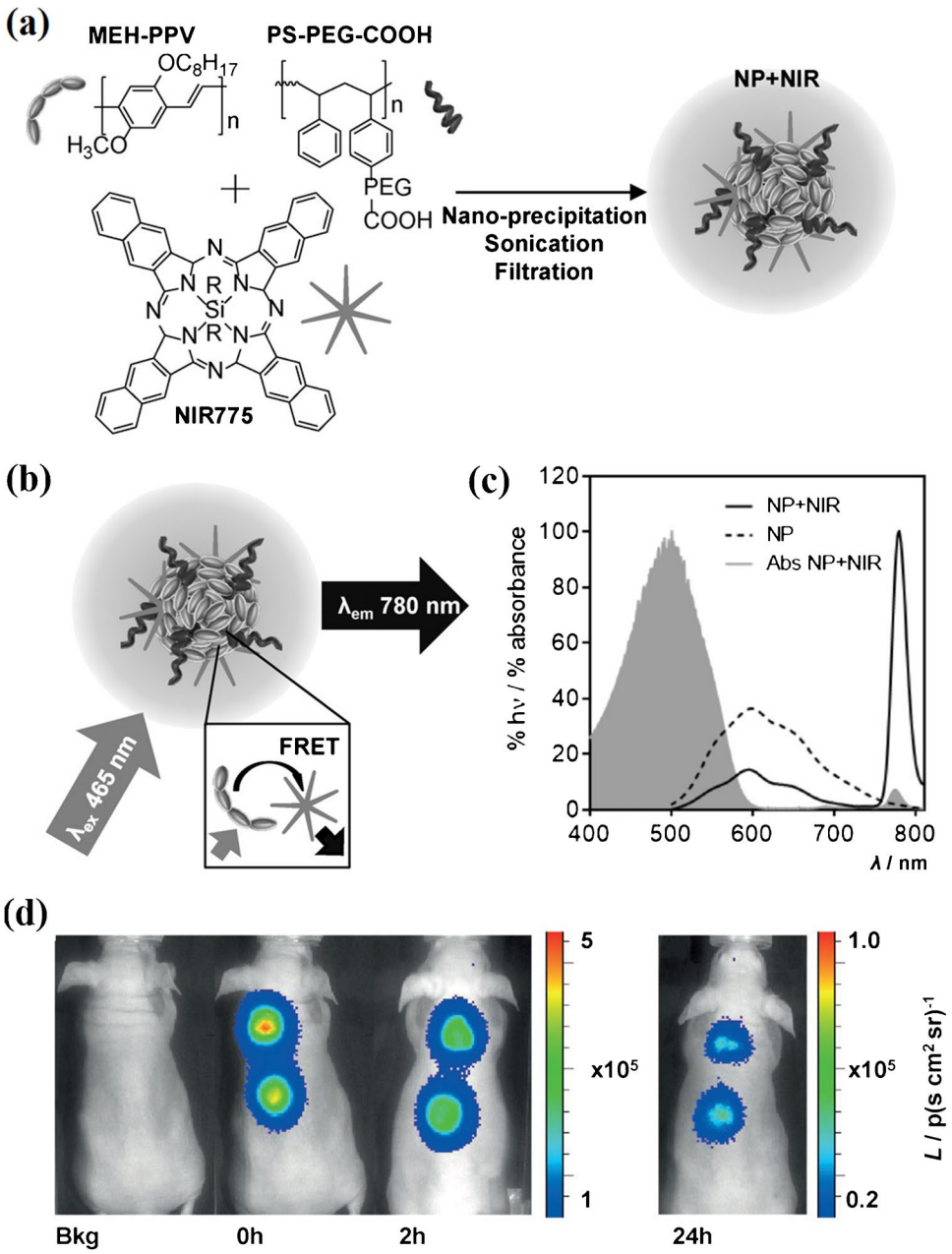

Fig. 17 (**a**) Preparation of NIR light emitting hybrid nanoparticles by nanoprecipitation of MEH-PPV, PS-PEG-COOH and NIR775. (**b**) Illustration of energy transfer from MEH-PPV to NIR775 through FRET mechanism for (**c**) augmenting the NIR emission of hybrid nanoparticles. (**d**) In vivo optical persistent imaging of mice after subcutaneous injection of hybrid nanoparticles. Reproduced with permission from reference [153]

hypoxia-responsive anticancer drug release. DOX/CP-NI nanoparticles were prepared through a double emulsion method using conjugated polymer CP-NI as a photosensitizer (grafted with 2-nitroimidazole (NI) as a hypoxia agent), polyvinyl PVA as a stabilizer and Dox as a cancer drug (Fig. 20a). The structure of CP-NI consists of dithiophene-thienopyrazine groups as a NIR imaging agent and dithiophene-benzotriazole moieties for producing ROS under visible/NIR light irradiation. Under the hypoxic environment, the NI exhibits tendency to be transformed into hydrophilic 2-aminoimidazole groups through a reduction reaction mediated by several nitroreductases and other enzymes typically found in the tissues. Thus, under NIR light (808 nm) irradiation and hypoxic condition, the DOX/CP-NI nanoparticles undergo dissociation and consequently release Dox into the cancer cells to achieve dual-responsive chemo- and PDT of cancer (Fig. 20b). The current technique offers an advanced strategy for attaining augmented treatment of cancer using a dual-responsive hybrid nanosystem. In order to evaluate the imaging-guided PDT ability of DOX/CP-NI NP, in vivo fluorescence images of HeLa tumor-bearing mice post intravenous delivery of DOX/CP-NI NPs was monitored after certain period of time (Fig. 20c). The results indicate strong fluorescence signal at the tumor sites compare to normal tissues and confirms the imaging-guided PDT capability of the system.

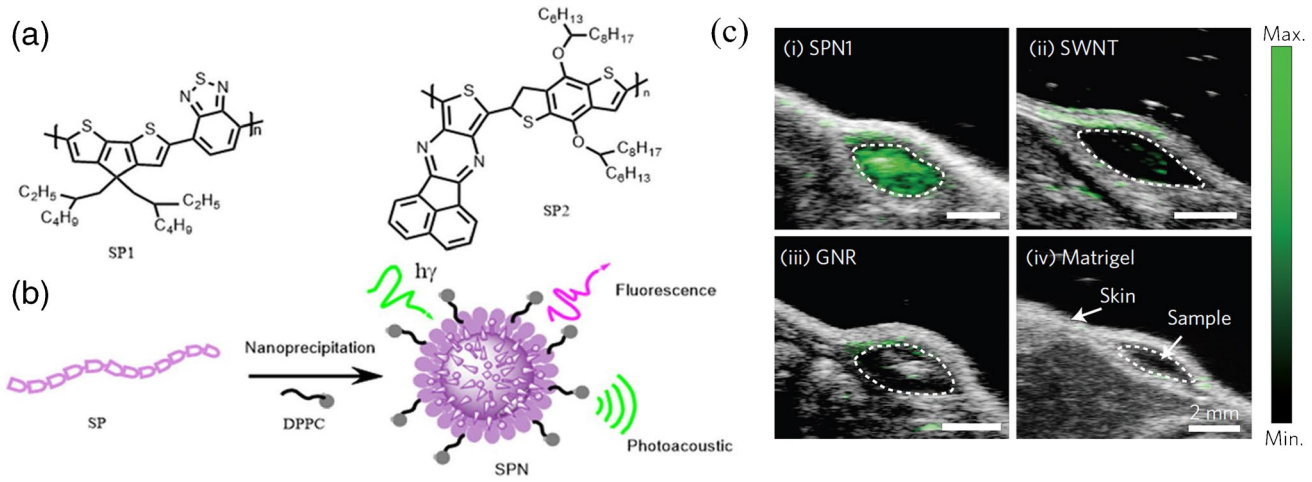

Fig. 18 (**a**) Structure of NIR light absorbing CPs (SP1 and SP2) and their (**b**) fabrication into corresponding nanoparticles (SPN = SPN1 and SPN2) through nanoprecipitation with DPPC. The nanoparticles displayed good photoacoustic and fluorescence signals under NIR laser irradiation. (**c**) Comparison of PA images of SP1 containing matrigel with GNRs, SWNTs and control matrigel inside the dorsal area of mice under laser pulse irradiation of 700 nm. Reproduced with permission from reference [158]

Rakovich and co-workers [175] reported two types of CPNs based on nanoprecipitation of CP PTB7(poly({4,8-bis[(2-ethylhexyl)oxy]benzo[1,2-b:4,5-b′]dithiophene-2,6-diyl}{3-fluoro-2-[(2-ethylhexyl)carbonyl]-thieno[3,4-b] thiophenediyl})) with PSMA and Pluronic F127, separately for bioimaging and PDT applications. Interestingly, PTB7@F127 NPs showed better photosensitizing property in contrast to PTB7@PSMA NPs confirming the crucial role of stabilizers in controlling the photosensitization property of CPNs.

Photothermal therapy (PTT)

Although PDT is among the pioneering methods discovered for non-invasive treatment of the diseases, yet, some drawbacks like its dependence on molecular oxygen and ultimately poor photodynamic efficacy in solid tumors remain as the major challenging issues for scientists. To overcome this issue, PTT [176–184] as an excellent therapeutic approach has gained much attention recently. Interestingly, photothermal agents absorb the light and convert the energy directly into heat through a non-radiative pathway without requiring molecular oxygen unlike in the case of PDT. The photothermal performance of any photothermal agent is usually evaluated by photothermal conversion efficiency (PCE) which is calculated by the well-known method [185]. Organic photothermal agents have made substantial progress in the therapeutic applications due to their superior biocompatibility and low toxicity compared to inorganic materials. Owing to this, several NIR-I light absorbing conjugated polymer materials have been reported

Table 2 CPNs and their nanohybrids for imaging applications

Conjugated polymer	Matrix	Size	λ_{ex}	λ_{em}	Application	Ref
P1-4	P1-4/PSMA	30 nm	360 nm	525 nm	In vitro imaging	120
MEH-PPV	MEH-PPV/m-THPC	~50 nm	480 nm	575 nm	In vitro imaging	128
P-F8-DPSB	P-F8-DPSB/DPA-PR-PDI	45 nm	800 nm	725 nm	In vitro imaging	135
PF-BT-DBT	PF-BT-DBT Pdots	36-41 nm	450 nm	725 nm	In vitro imaging	136
P2	P2 Pdots	5 nm	405 nm	656 nm	In vitro imaging	141
MEH-PPV	MEH-PPV/cRGD	~35 nm	495 nm	585 nm	In vitro imaging	146
PCLA-$O_2^{\bullet-}$	PCLA-$O_2^{\bullet-}$ NPs	20 nm	-	570 nm	In vivo imaging	150
MEH-PPV	MEH-PPV/PS-PEG-COOH	20–50 nm	729 nm	780 nm	In vivo imaging	153
SP1 and SP2	SP/DPPC	~40 nm	680 nm	838 nm	In vivo imaging	158
PFBT	PFBT/PS-PEG-COOH/IONPs	140–146 nm	460 nm	540 nm	In vivo imaging	152
PFTBT	^{S}SiO2@^{S}PFTBT@$^{C}SiO_2$	55.7 nm	561 nm	702 nm	In vivo imaging	154
TTQ-2TC	TTQ-2TC/PS-PEG	140 nm	~808 nm	~1270 nm	In vivo imaging	155
PBDP-DPP	PBDP-DPP/BSA	5 nm	790 nm	790 nm	In vivo imaging	159

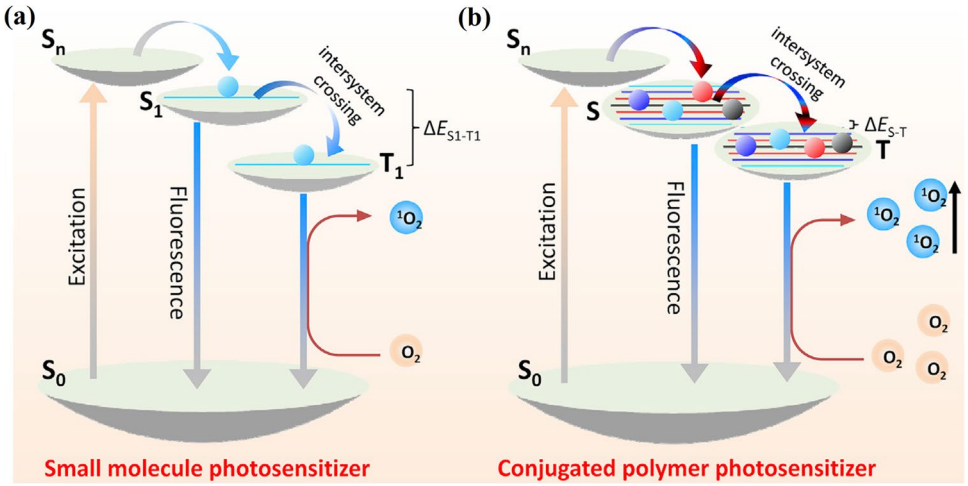

Fig. 19 Mechanistic pathway of the generation of $^1O_2$ by (**a**) small molecule and (**b**) CP as photosensitizer. Reproduced with permission from reference [161]

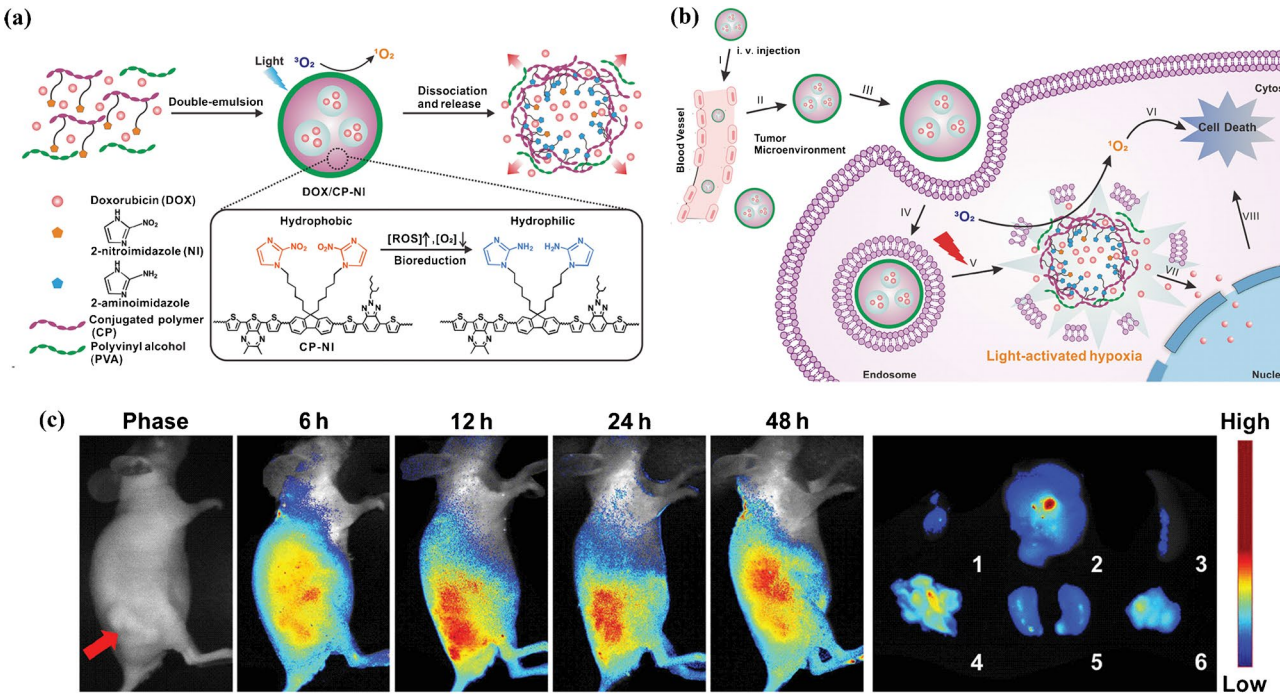

Fig. 20 (**a**) Structure of CP-NI and its fabrication into Dox loaded dual-responsive DOX/CP-NI nanoparticles via double-emulsion method. (**b**) Schematic of light mediated hypoxia and subsequent release of Dox into cancer cells for chemotherapy along with PDT. (**c**) In vivo fluorescence images of HeLa tumor-bearing mice post intravenous delivery of DOX/CP-NI NPs and after certain period of time indicating strong signal at tumor sites. After laser irradiation for 5 min at the tumor sites 48 postadministration of nanoparticles, the decreased fluorescence intensity was observed confirming imaging-guided PDT capability of the system. Reproduced with permission from reference [174]

as efficient photothermal agents [186–194]. However, the designing and development of CPN-based organic photothermal materials with the absorption in NIR-II biological window (1000–1700 nm) for deep tissue penetration and minimal scattering are highly desirable but scarcely reported [195–198] and scientists are continuously putting their efforts for further advancements.

For example, Deng et al. [199] synthesized a new NIR-I light-absorbing CP (DPP-BDP) via Stille cross-coupling reaction. Using pluronic F127 as a stabilizer and FA as a targeting unit, DPP-BDP was fabricated into corresponding nanoparticles (DB-FA NPs) of uniform size (200 nm) via simple emulsion method with exceptional PCE of 38.9% under NIR light (808 nm) excitation (Fig. 21a). The

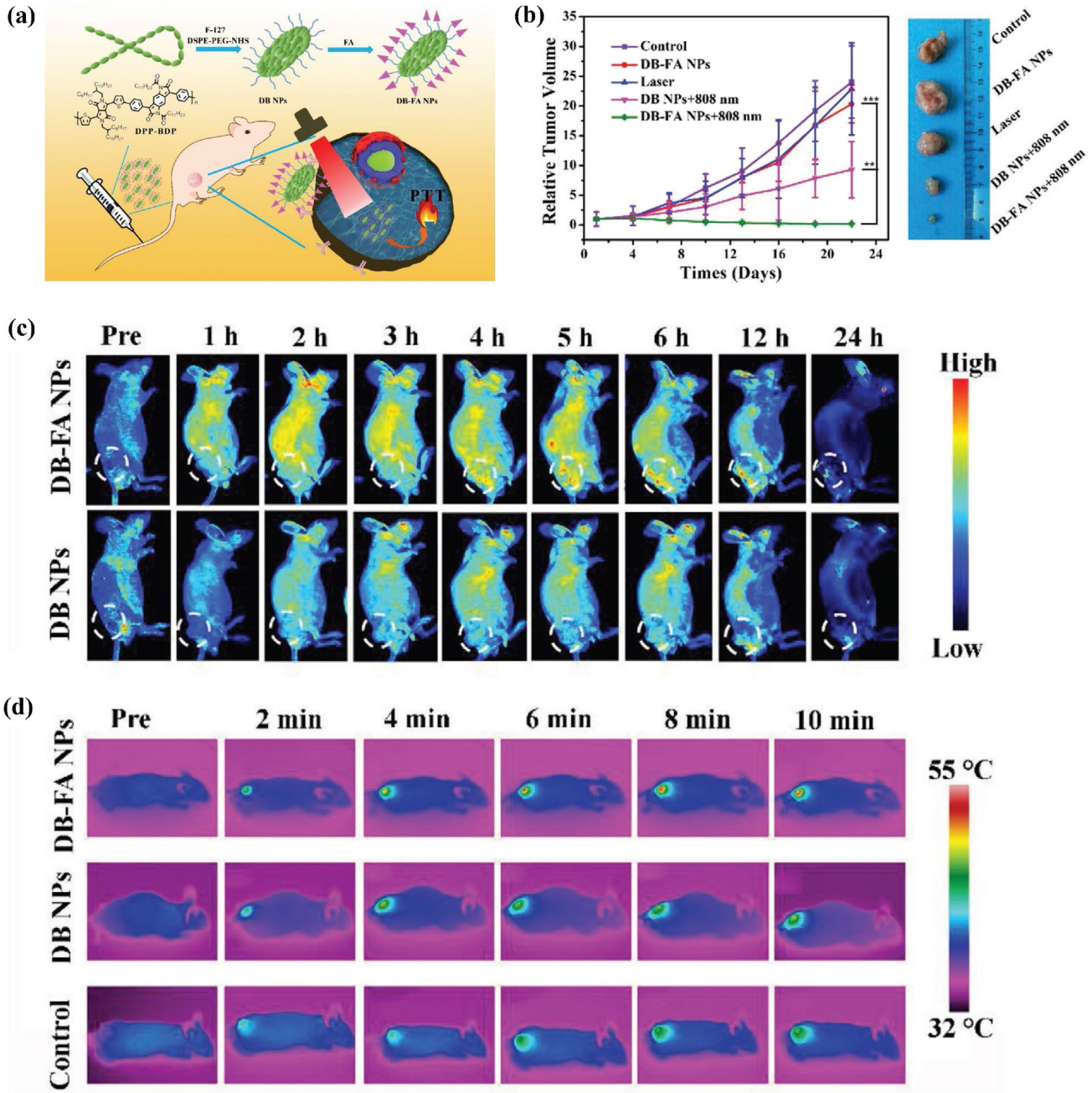

Fig. 21 (**a**) Fabrication of NIR-I light absorbing DB-FA NPs via simple emulsion method for PTT application and (**b**) its anti-tumor activity in vivo. (**c**) In vivo fluorescence images of BALB/c mice pre and post injection of DB-Cy3 and DB-FA/Cy3 nanoparticles at different time intervals. The mice injected with DB-FA/Cy3 nanoparticles showed strong fluorescence signal at the tumor site. (**d**) IR thermal images of BALB/c mice pre and post injection of DB-Cy3 and DB-FA/Cy3 nanoparticles under NIR laser (808 nm, 1 W cm^{-2}) irradiation at different time intervals. Control group contain only phosphate buffer saline (PBS). Reproduced with permission from reference [199]

as-prepared DB-FA NPs demonstrated an outstanding anticancer activity both in vitro and in vivo via PTT under NIR-I (808 nm) laser irradiation (0.8 W cm^{-2} or 1 W cm^{-2}). Nearly 99.2% reduction in the size of tumor was observed after injecting DB-FA NPs in the tumor-bearing mice (Fig. 21b) asserting the ability of designed nanosytem in high-efficient PTT of solid-state tumors. To confirm the potential of DB-FA nanoparticles in targeted therapy, in vivo imaging studies were performed using BALB/c mice injected separately with DB-Cy3 and DB-FA/Cy3 nanoparticles (Fig. 21c). Moreover, the photothermal effect monitored by IR thermal imaging technique in tumor xenografts of nude

mice also confirmed targeting PTT ability of DF-FA nanoparticles (Fig. 21d). Liu and co-workers [40] also reported synthesis of a new NIR-I CP poly[9,9-bis(4-(2-ethylhexyl) phenyl)fluorene-alt-co-6,7-bis(4-(hexyloxy)phenyl)-4,9-di(thiophen-2-yl)-thiadiazoloquinoxaline] (PFTTQ) and its fabrication into corresponding PFTTQ nanoparticles via precipitation method. Under NIR-I (808 nm) laser irradiation (0.75 W/cm^{-2}) for about 5 min, the suspension of PFTTQ nanoparticles displayed an increment in the temperature of > 30 °C and demonstrate sensible photothermal therapy efficiency both in cancer cells as well as in tumor mouse model.

PTT in the first NIR (NIR-I, 750–1000 nm) optical window has been adequately studied over the last few decades [200]. Recently, photothermal conversion in the second NIR (NIR-II, 1000–1700 nm) optical window, particularly within the range of 1000–1100 nm has received much attention because it allows deeper tissue penetration and the usage of high power laser [201]. Xie et al. [196] designed a NIR-II photothermal nanoagent based on a narrow band-gap donor–acceptor CP (TBDOPV-DT) with 2,2-bithiophene as the donor and thiophene-fused benzodifurandione-based oligo(*p*-phenylenevinylene) as the receptor. The CP was transformed into TBDOPV-DT NPs via nanoprecipitation with methoxypoly(ethylene glycol)$_{2\ K}$-*block*-poly($_{D,L}$-lactide)$_{2\ K}$ (mPEG$_{2K}$-PDLLA$_{2K}$) (Fig. 22a) and demonstrate excellent capability for photoacoustic imaging (PAI) guided PTT under NIR-II (1064 nm) laser irradiation. PAI was accomplished after intravenous injection of TBDOPV-DT NPs inside HeLa-tumor bearing mice which indicate strong PA signal which retain upto 12 h post injection (Fig. 22b, c). The PCE of TBDOPV-DT NPS was calculated to be 50% with extraordinary photostability and thermal reproducibility. IR thermal images of TBDOPV-DT NPs injected mice model showed rapid increment of temperature under NIR-II laser (1064 nm) irradiation (Fig. 22d). In particular, the nanoparticles displayed an efficient PTT effect in-vitro in cancer cells and also eliminate tumor cells completely in vivo with no significant side effects. Another NIR-II light-absorbing CP TT-BTT-BBT was designed and synthesized

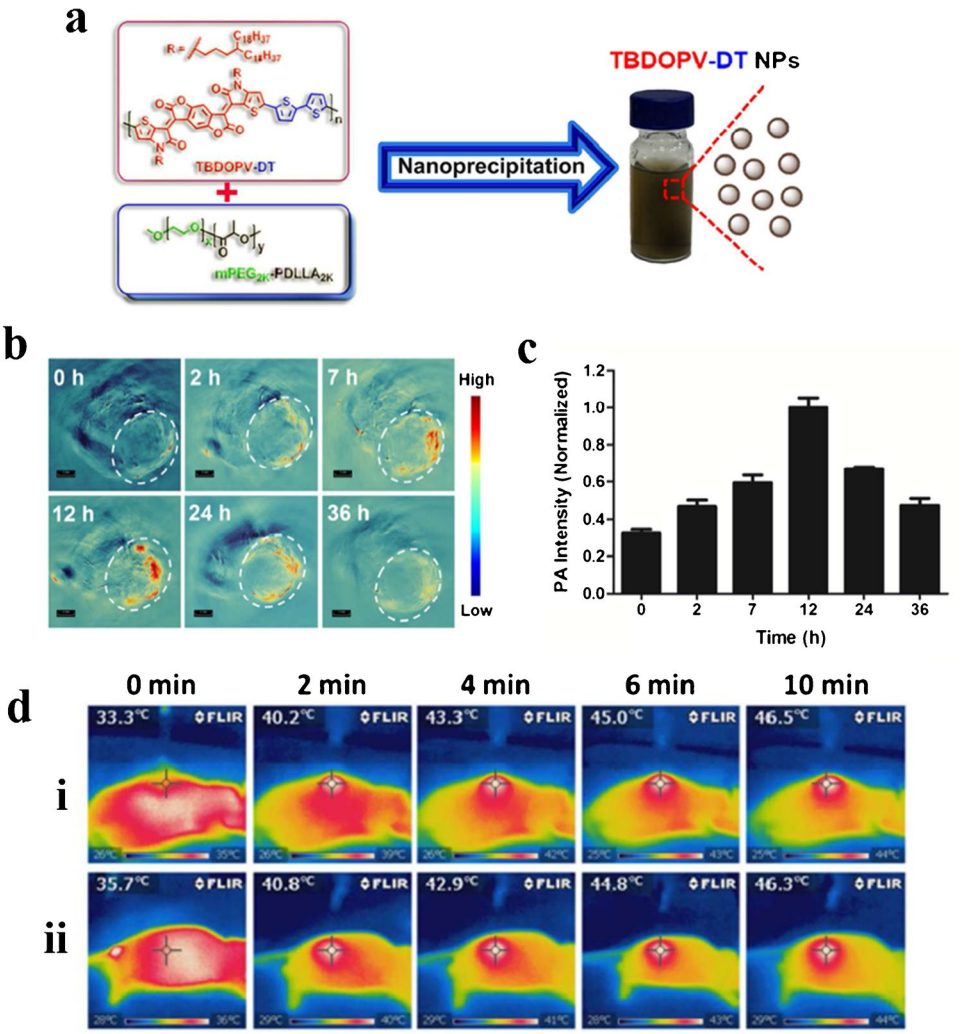

Fig. 22 (**a**) Preparation of spherical TBDOPV-DT NPs via nanoprecipitation of CP TBDOPV-DT with mPEG$_{2K}$-PDLLA$_{2K}$. (**b**) Photoacoustic (PA) images under 1064 nm laser illumination and (**c**) intensities of signal obtained at different time intervals after injection of TBDOPV-DT NPs inside HeLa-tumor bearing nude mice. Strongest PA signal was obtained after 12 h post injection. (**d**) IR thermal images of HeLa-tumor bearing mice under 1064 nm laser illumination after (i) intratumoral and (i) intravenous injection of TBDOPV-DT NPs at different time. Reproduced with permission from reference [196]

by the same group [195] and fabricated into nanoparticles using Pluronic F127 as encapsulating material. The photothermal conversion behavior and PTT effect of acquired nanoparticles were studied by NIR-II (1064 nm) laser using NIR-I (808 nm) laser as the control. The results confirmed that under the same conditions, NIR-II laser showed more effective inhibition of hepatocellular carcinoma in situ and remain superior for the proficient treatment of liver cancer.

Drug delivery

Drug delivery is the process of delivering pharmaceutical compounds into the body using career molecules like dendrimers, liposomes, self-assembling peptides, polymeric micelles, nanostructures and so on. The size of the drug molecule and the amount of loading are the two main parameters that regulate the drug delivery mechanism. The confined targeting, low therapeutic indices, poor water solubility, etc. are the major challenges in designing the drug delivery systems. Owing to low cytotoxicity, sustainable release of drug through various stimuli responsive mechanisms and its monitoring via fluorescence imaging, CPNs have gained much prominence in the field of drug delivery [17, 20, 202–206].

Iyer et al. [126] reported the fabrication of multifunctional and dual-emissive CPNs using hydroxyquinoline-affixed polyfluorene (PF-HQ) derivative for bioimaging applications as well as delivery of drug inside the cancer cells. Compare to free Dox, Dox loaded PF-HQ nanoparticles displayed enhanced anti-cancer activity towards mouse melanoma cancer cells (B16F10) and subcutaneous mouse (C57BL6/J) melanoma tumor model. However, this system lacks specificity as no receptors were appended for targeted imaging and delivery of drug inside the cancer cells. In 2018, Liu and coworkers [207] synthesized a FA and donor–acceptor Stenhouse adduct (DASA) functionalized CP (PPV-ST) and fabricated into drug loaded photo-responsive CPNs via nanoprecipitation method for achieving controlled drug delivery, release and imaging (Fig. 23). Unlike PF-HQ nanoparticles, this nanoprobe could facilitate light triggered controlled delivery of drug inside the cancer cells and monitor its release via imaging. The photo-responsive CPNs comprise of three main parts: the photo-responsive group, conjugated backbone, and the receptor moiety (Fig. 23a). Under irradiation of visible light (550 nm), the as-prepared CPNs experience the change in shape, color, polarity and ultimately release the encapsulated drug into the cancer cells (Fig. 23b). Under dark conditions, the drug loaded CPNs displayed outstanding biocompatibility towards the cancer cells which affirmed that the light trigger has full control over drug release. Moreover, the delivery of both hydrophilic

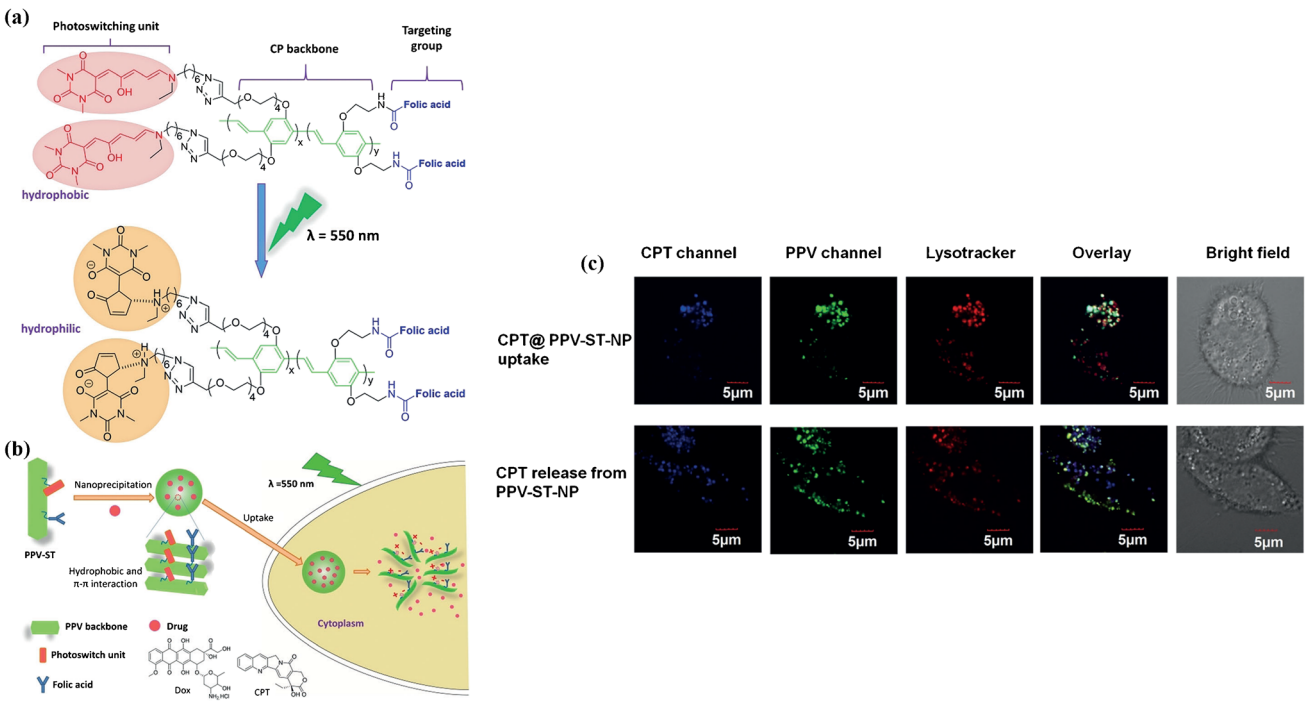

Fig. 23 (**a**) Structure of newly prepared photo-responsive CP PPV-ST bearing photoswitchable groups and targeting units. The photoswitchable groups attached to PPV-ST undergo change in its structure from open to closed form under irradiation of visible light (550 nm). (**b**) The photoresponsive CPNs were formed through nanoprecipitation of PPV-ST with PSMA followed by encapsulation of cancer drugs (Dox and CPT). Drug-loaded CNPs was uptake by cancer cells and the drug was released in a controlled manner under visible light irradiation (550 nm). (**c**) The uptake of CPT loaded nanoparticles and subsequent release of CPT was monitored inside HeLa cells by confocal laser scanning microscopy (CLSM). Reproduced with permission from reference [207]

(Dox) and hydrophobic (camptothecin (CPT)) drugs could be realized with high loading efficiency. The uptake of nanoparticles and subsequent release of drug was successfully examined inside HeLa cancer cells by fluorescence imaging studies (Fig. 23c). The designed approach with a remote-controlled drug delivery using visible light irradiation sets a precedent for non-invasive therapeutic delivery of careers.

Compare to single mode therapeutic method, combination of two methods is always beneficial for accomplishing synergistic anti-cancer activity. In 2019, Tang and co-workers [208] reported the preparation of thermal-responsive nano drug delivery system (PNIPAM-DOX-CPNs) via co-assembly of CP poly(fluorene-co-vinylene) (PFV) with temperature-sensitive molecule PNIPAM and the Food and Drug Administration (FDA) approved anticancer drug Dox for accomplishing synergistic chemo-photodynamic therapy of cancer (Fig. 24a). PNIPAM-DOX-CPNs nanoparticles demonstrate a variety of functions including the cell imaging, thermo-responsive drug delivery and synergistic therapy of cancer via chemo/photodynamic treatment. The dispersion of PNIPAM-DOX-CPNs at pH of 5.5 and a temperature of 36 °C indicate > 70% delivery of the loaded Dox inside the cancer (MCF-7) cells which suggests that the drug is delivered effectively above PNIPAM's lower critical solution temperature (LCST). The bright green emission of nanoparticles allows successful monitoring of drug release via fluorescent imaging technique (Fig. 24b). Moreover, under white light irradiation, PFV in nanoparticles acted as a photosensitizer and produce effective ROS, resulting in synergistic chemo/photodynamic therapy.

The above discussed papers related to theranostic applications of CPNs and their nanohybrids are summarized in Table 3.

Conclusion and perspectives

Conjugated polymer nanoparticle (CPNs) with outstanding photophysical properties has emerged as a revolutionary material for variable biological and biomedical applications. This review comprehensively introduces CPNs, highlighted their methods of preparation and described their state-of-art advances in biological sensing, imaging, diagnosis, and therapy taking cancer as a disease model. Compared with other class of organic/inorganic nanomaterials, CPNs exhibits several advantages as outlined in the following text. (1) Preparation of surface-modified CPNs is simple with an easy separation process. (2) They possess excellent fluorescence quantum yield, low cytotoxicity and excellent photostability. (3) They display high-sensitivity and rapid fluorescence signal response towards desired sensing analyte owing to the phenomenon of molecular-wire effect [8, 150] typically observed in conjugated polymer material. (4) Reactive oxygen species (ROS) generation ability and photothermal conversion efficiency (PCE) of CPNs required for proficient photodynamic (PDT) and photothermal therapy (PTT) are considerably higher. These features make CPNs and their nanohybrids as preferred choice of nanomaterials for variety of applications.

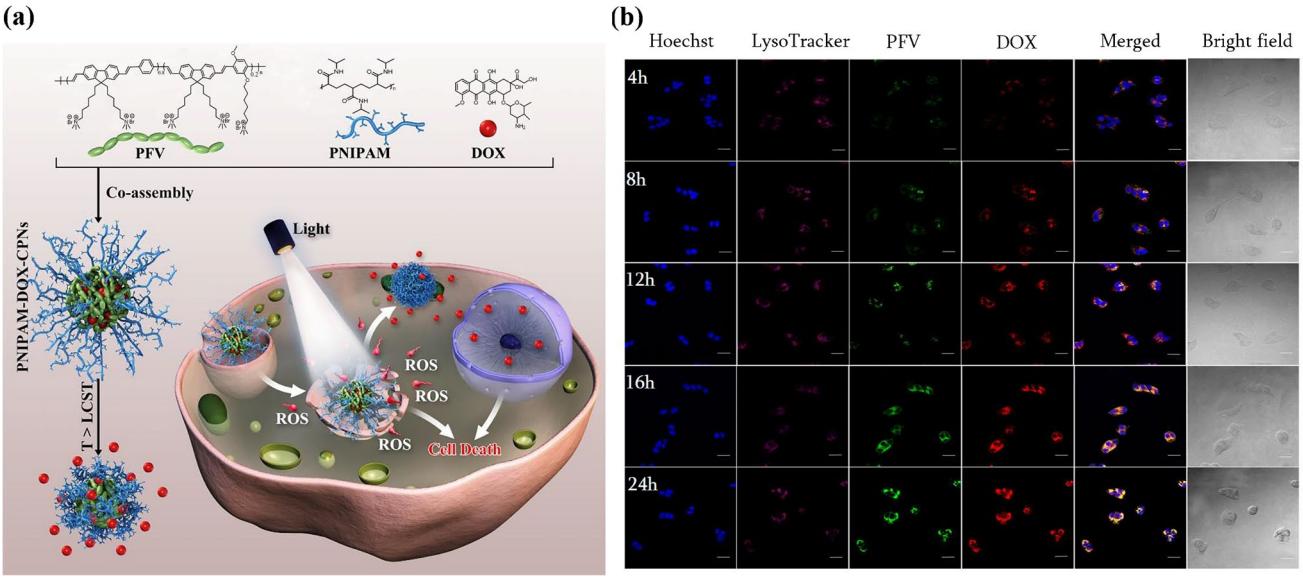

Fig. 24 (**a**) Fabrication procedure of thermo-responsive PNIPAM-DOX-CPNs loaded with Dox via co-assembly method for application in drug delivery and synergistic chemo/photodynamic treatment of cancer. (**b**) CLSM images of MCF-7 cancer cells after incubation with PNIPAM-DOX-CPNs (5 μg/mL) for different time intervals. Cell uptake of nanoparticles and release of drug was tracked by monitoring green emission of PNIPAM-DOX-CPNs and red emission of Dox at different time intervals. Lysotracker red DND 99 and Hoechst 33342 were employed to stain lysosomes and nucleus, respectively. Reproduced with permission from reference [208]

Table 3 CPNs and their nanohybrids for theranostic applications

Conjugated polymer	Matrix	Size	Light Irradiation	PCE	Application	Ref
CP-NI	CP-NI/DOX	~120 nm	488 nm	NA	Imaging-guided in vivo PDT	174
PTB7	PTB7@F127	~190 nm	635 nm	NA	Imaging and PDT	175
DPP-BDP	DPP-BDP/FA/F127	~200 nm	808 nm	38.9%	IR thermal imaging and PTT	199
PFTTQ	PFTTQ/DSPE-PEG_{2000}	25 nm	808 nm	-	IR thermal imaging and PTT	40
TBDOPV-DT	TBDOPV-DT/ $mPEG_{2K}$-$PDLLA_{2K}$	~170 nm	1064 nm	50%	PAI-guided PTT	196
PF-HQ	PF-HQ/DOX	~225 nm	-	NA	Imaging and drug delivery	126
PPV-ST	PPV-ST/PSMA	80 nm	550 nm	NA	Drug delivery and tracking	207
PFV	PNIPAM-DOX-CPNs	~90 nm	400–700 nm	NA	Drug delivery, tracking and PDT	208

Nevertheless, the exciting progress has been made in the area of CPNs, following limitations and challenges still exist. (1) The preparation of CPNs with a uniform size is slightly difficult compare to inorganic nanomaterials such as metal nanoparticles. (2) The aggregation-caused quenching (ACQ) effect in an aqueous solution due to strong hydrophobicity of CP material radically affects photophysical properties (e.g. fluorescence brightness), sensing performance and ROS production of CPNs. (3) For targeted imaging and therapeutic applications in vivo, CPNs still suffer from the issue of selectivity, since their distribution to other organs could not be evaded. (4) Fabrication of long-wavelength absorbing CPNs especially in near-infrared II (NIR-II) window for effective PDT and PTT is rigorous. Thus, there is plenty of space for scientists to circumvent the existing challenges and develop high performance CPNs through innovative pathways.

Thus, the future designing and development of CPNs-based probes should consider and focus on the following aspects. (1) Fabrication of target-specific CPNs with emission in longer wavelength in order to avoid photo bleaching and toxicity effects during sensing and drug-delivery applications. (2) Preparation of aggregation-induced emission (AIE)-active CPs and corresponding CPNs via simplified route with improved bioimaging and PDT performance. (3) Designing of new types of donor–acceptor CPs and relevant CPNs with better dispersibility in an aqueous solution for augmented PDT and PTT performance. It is anticipated that through the collective efforts of various investigators, the area of CPNs will be cultivated further with wider application prospects and the findings summarized in this review may be helpful to them and other relevant audiences.

Funding Financial support from National Natural Science Foundation of China (Nos. 21305107, 81701830), the Natural Science Foundation of Shaanxi Province (Nos. 2020JM-066, 2020JQ-019), the Fundamental Research Funds for the Central Universities (Nos. xjh012020001, xjj2017028) and China Postdoctoral Science Foundation (No. 2020M673368) is gratefully acknowledged.

Declarations

Conflict of interest The authors declare no competing interests.

References

1. Shirakawa H, Louis EJ, MacDiarmid AG, Chiang CK, Heeger AJ (1977) Synthesis of electrically conducting organic polymers: halogen derivatives of polyacetylene, (CH). J Chem Soc Chem Commun 1977:578–580. https://doi.org/10.1039/C39770000578
2. Swager TM (2017) 50th Anniversary Perspective: Conducting/Semiconducting Conjugated Polymers. A Personal Perspective on the Past and the Future. Microchim Acta 50:4867–4886. https://doi.org/10.1021/acs.macromol.7b00582
3. He Y, Hu X, Gong Z, Chen S, Yuan R (2020) A novel electrochemiluminescence biosensor based on the self-ECL emission of conjugated polymer dots for lead ion detection. Microchim Acta 187:237. https://doi.org/10.1007/s00604-020-4212-0
4. Liu Y, Yan H, Shangguan J, Yang X, Wang M, Liu W (2018) A fluorometric aptamer-based assay for ochratoxin A using magnetic separation and a cationic conjugated fluorescent polymer. Microchim Acta 185:427. https://doi.org/10.1007/s00604-018-2962-8
5. Hussain S, Zhao H, Zhou L, Zhou X, Iyer PK, Lv F, Liu L, Wang S (2019) An Optoelectronic Device for Rapid Monitoring of Creatine Kinase Using Cationic Conjugated Polyelectrolyte. Adv Mater Technol 4:1900361. https://doi.org/10.1002/admt.201900361
6. Hussain S, Lv F, Qi R, Senthilkumar T, Zhao H, Chen Y, Liu L, Wang S (2020) Förster Resonance Energy Transfer Mediated Rapid and Synergistic Discrimination of Bacteria over Fungi Using a Cationic Conjugated Glycopolymer. ACS Appl Bio Mater 3:20–28. https://doi.org/10.1021/acsabm.9b00691
7. Hussain S, Malik AH, Iyer PK (2016) FRET-assisted selective detection of flavins via cationic conjugated polyelectrolyte under physiological conditions. J Mater Chem B 4:4439–4446. https://doi.org/10.1039/C6TB01350C
8. Rochat S, Swager TM (2013) Conjugated Amplifying Polymers for Optical Sensing Applications. ACS Appl Mater Interfaces 5:4488–4502. https://doi.org/10.1021/am400939w
9. Coakley KM, McGehee MD (2004) Conjugated Polymer Photovoltaic Cells. Chem Mater 16:4533–4542. https://doi.org/10.1021/cm049654n
10. Dwivedi AK, Saikia G, Iyer PK (2011) Aqueous polyfluorene probe for the detection and estimation of Fe^{3+} and inorganic phosphate in blood serum. J Mater Chem 21:2502–2507. https://doi.org/10.1039/C0JM03054F

11. Yu K, Park B, Kim G, Kim CH, Park S, Kim J, Jung S, Jeong S, Kwon S, Kang H, Kim J, Yoon MH, Lee K (2016) Optically transparent semiconducting polymer nanonetwork for flexible and transparent electronics. Proc Natl Acad Sci 113:14261. https://doi.org/10.1073/pnas.1606947113
12. Hussain S, Malik AH, Afroz MA, Iyer PK (2015) Ultrasensitive detection of nitroexplosive – picric acid via a conjugated polyelectrolyte in aqueous media and solid support. Chem Commun 51:7207–7210. https://doi.org/10.1039/C5CC02194D
13. Hussain S, Malik AH, Iyer PK (2015) Highly Precise Detection, Discrimination, and Removal of Anionic Surfactants over the Full pH Range via Cationic Conjugated Polymer: An Efficient Strategy to Facilitate Illicit-Drug Analysis. ACS Appl Mater Interfaces 7:3189–3198. https://doi.org/10.1021/am507731t
14. Pecher J, Mecking S (2010) Nanoparticles of Conjugated Polymers. Chem Rev 110:6260–6279. https://doi.org/10.1021/cr100132y
15. Tuncel D, Demir HV (2010) Conjugated polymer nanoparticles Nanoscale 2:484–494. https://doi.org/10.1039/B9NR00374F
16. Meher N, Iyer PK (2017) Pendant chain engineering to fine-tune the nanomorphologies and solid state luminescence of naphthalimide AIEEgens: application to phenolic nitro-explosive detection in water. Nanoscale 9:7674–7685. https://doi.org/10.1039/C7NR02174G
17. Feng L, Zhu C, Yuan H, Liu L, Lv F, Wang S (2013) Conjugated polymer nanoparticles: preparation, properties, functionalization and biological applications. Chem Soc Rev 42:6620–6633. https://doi.org/10.1039/C3CS60036J
18. Wang Y, Feng L, Wang S (2019) Conjugated Polymer Nanoparticles for Imaging, Cell Activity Regulation, and Therapy. Adv Funct Mater 29:1806818. https://doi.org/10.1002/adfm.201806818
19. Jiang Y, McNeill J (2017) Light-Harvesting and Amplified Energy Transfer in Conjugated Polymer Nanoparticles. Chem Rev 117:838–859. https://doi.org/10.1021/acs.chemrev.6b00419
20. Sarkar S, Levi-Polyachenko N (2020) Conjugated polymer nanosystems for hyperthermia, imaging and drug delivery. Adv Drug Delivery Rev 163–164:40–64. https://doi.org/10.1016/j.addr.2020.01.002
21. Liu Y, Wu P, Jiang J, Wu J, Chen Y, Tan Y, Tan C, Jiang Y (2016) Conjugated Polyelectrolyte Nanoparticles for Apoptotic Cell Imaging. ACS Appl Mater Interfaces 8:21984–21989. https://doi.org/10.1021/acsami.6b09347
22. Li K, Ding D, Huo D, Pu KY, Thao NNP, Hu Y, Li Z, Liu B (2012) Conjugated Polymer Based Nanoparticles as Dual-Modal Probes for Targeted In Vivo Fluorescence and Magnetic Resonance Imaging. Adv Funct Mater 22:3107–3115. https://doi.org/10.1002/adfm.201102234
23. Cui H, Chen Y, Li L, Wu Y, Tang Z, Fu H, Tian Z (2014) Hybrid fluorescent nanoparticles fabricated from pyridine-functionalized polyfluorene-based conjugated polymer as reversible pH probes over a broad range of acidity-alkalinity. Microchim Acta 181:1529–1539. https://doi.org/10.1007/s00604-014-1219-4
24. Clement S, Chen W, Anwer AG, Goldys EM (2017) Verteporfin conjugated to gold nanoparticles for fluorescent cellular bioimaging and X-ray mediated photodynamic therapy. Microchim Acta 184:1765–1771. https://doi.org/10.1007/s00604-017-2145-z
25. Wu C, Chiu DT (2013) Highly Fluorescent Semiconducting Polymer Dots for Biology and Medicine. Angew Chem Int Ed 52:3086–3109. https://doi.org/10.1002/anie.201205133
26. Di Benedetto F, Camposeo A, Pagliara S, Mele E, Persano L, Stabile R, Cingolani R, Pisignano D (2008) Patterning of light-emitting conjugated polymer nanofibres. Nat Nanotechnol 3:614–619. https://doi.org/10.1038/nnano.2008.232
27. Kelly TL, Wolf MO (2010) Template approaches to conjugated polymer micro- and nanoparticles. Chem Soc Rev 39:1526–1535. https://doi.org/10.1039/B914333P
28. Lei W, Si W, Xu Y, Gu Z, Hao Q (2014) Conducting polymer composites with graphene for use in chemical sensors and biosensors. Microchim Acta 181:707–722. https://doi.org/10.1007/s00604-014-1160-6
29. Gao D, Hu D, Liu X, Zhang X, Yuan Z, Sheng Z, Zheng H (2020) Recent Advances in Conjugated Polymer Nanoparticles for NIR-II Imaging and Therapy. ACS Appl Mater Interfaces 2:4241–4257. https://doi.org/10.1021/acsapm.0c00679
30. MacFarlane LR, Shaikh H, Garcia-Hernandez JD, Vespa M, Fukui T, Manners I (2021) Functional nanoparticles through π-conjugated polymer self-assembly. Nat Rev Mater 6:7–26. https://doi.org/10.1038/s41578-020-00233-4
31. Dalkiran B, Brett CMA (2021) Polyphenazine and polytriphenylmethane redox polymer/nanomaterial–based electrochemical sensors and biosensors: a review. Microchim Acta 188:178. https://doi.org/10.1007/s00604-021-04821-1
32. Stanley A, Subash CBG (2018) Polymer Conjugated Gold Nanoparticles in Biomedical Applications. Curr Med Chem 25:1433–1445. https://doi.org/10.2174/0929867324666170116123633
33. Schanze KS (2004) Organometallic Conjugation: Structures, Reactions and Functions of d−d and d−π Conjugated Systems Edited by Akira Nakamura, Norikazu Ueyama, and Kizashi Yamaguchi (Osaka University). From the Series: Chemical Physics, Volume 73. Kodansha, Ltd: Tokyo. Springer-Verlag: Berlin, Heidelberg, New York. 2002. xvi + 352 pp. $129.00. Kodansha ISBN 4–06–209654–4. Springer-Verlag ISBN 3–540–00088–7. J Am Chem Soc 126: 408–408. https://doi.org/10.1021/ja033547x
34. Chen X, Hussain S, Hao Y, Tian X, Gao R (2021) Review—Recent Advances of Signal Amplified Smart Conjugated Polymers for Optical Detection on Solid Support. ECS J Solid State Sci Technol 10:037006. https://doi.org/10.1149/2162-8777/abeed1
35. Liu B, Wang S, Bazan GC, Mikhailovsky A (2003) Shape-Adaptable Water-Soluble Conjugated Polymers. J Am Chem Soc 125:13306–13307. https://doi.org/10.1021/ja0365072
36. Zhu C, Yang Q, Liu L, Wang S (2011) A potent fluorescent probe for the detection of cell apoptosis. Chem Commun 47:5524–5526. https://doi.org/10.1039/C0CC05158F
37. Moon JH, McDaniel W, MacLean P, Hancock LF (2007) Live-Cell-Permeable Poly(p-phenylene ethynylene). Angew Chem Int Ed 46:8223–8225. https://doi.org/10.1002/anie.200701991
38. Neo WT, Ye Q, Shi Z, Chua SJ, Xu J (2018) Influence of catalytic systems in Stille polymerization on the electrochromic performance of diketopyrrolopyrrole-based conjugated polymers. Mater Chem Front 2:331–337. https://doi.org/10.1039/c7qm00377c
39. Albernaz VL, Bach M, Weber A, Southan A, Tovar GEM (2018) Active Ester Containing Surfmer for One-Stage Polymer Nanoparticle Surface Functionalization in Mini-Emulsion Polymerization. Polymers 10:408. https://doi.org/10.3390/polym10040408
40. Li K, Pan J, Feng SS, Wu AW, Pu KY, Liu Y, Liu B (2009) Generic Strategy of Preparing Fluorescent Conjugated-Polymer-Loaded Poly(DL-lactide-co-Glycolide) Nanoparticles for Targeted Cell Imaging. Adv Funct Mater 19: liu-3542. https://doi.org/10.1002/adfm.200901098
41. Howes P, Green M, Levitt J, Suhling K, Hughes M (2010) Phospholipid Encapsulated Semiconducting Polymer Nanoparticles: Their Use in Cell Imaging and Protein Attachment. J Am Chem Soc 132:3989–3996. https://doi.org/10.1021/ja1002179
42. Chen J, Wang D, Turshatov A, Muñoz-Espí R, Ziener U, Koynov K, Landfester K (2013) One-pot fabrication of amphiphilic photoswitchable thiophene-based fluorescent polymer dots. Polym Chem 4:773–781. https://doi.org/10.1039/C2PY20589K

43. Yan C, Sun Z, Guo H, Wu C, Chen Y (2017) Thiophene-fused 1,10-phenanthroline toward a far-red emitting conjugated polymer and its polymer dots: synthesis, properties and subcellular imaging. Mater Chem Front 1:2638–2642. https://doi.org/10.1039/C7QM00379J
44. Piwoński H, Michinobu T, Habuchi S (2017) Controlling photophysical properties of ultrasmall conjugated polymer nanoparticles through polymer chain packing. Nat Commun 8:15256. https://doi.org/10.1038/ncomms15256
45. Yang J, Wu D, Xie D, Feng F, Schanze KS (2013) Ion-Induced Aggregation of Conjugated Polyelectrolytes Studied by Fluorescence Correlation Spectroscopy. J Phys Chem B 117:16314–16324. https://doi.org/10.1021/jp408370e
46. Wang C-W, Sinton D, Moffitt MG (2011) Flow-Directed Block Copolymer Micelle Morphologies via Microfluidic Self-Assembly. J Am Chem Soc 133:18853–18864. https://doi.org/10.1021/ja2067252
47. Wang G, Persson N, Chu PH, Kleinhenz N, Fu B, Chang M, Deb N, Mao Y, Wang H, Grover MA, Reichmanis E (2015) Microfluidic Crystal Engineering of π-Conjugated Polymers. ACS Nano 9:8220–8230. https://doi.org/10.1021/acsnano.5b02582
48. Huang Y, Moini Jazani A, Howell EP, Oh JK, Moffitt MG (2020) Controlled Microfluidic Synthesis of Biological Stimuli-Responsive Polymer Nanoparticles. ACS Appl Mater Interfaces 12:177–190. https://doi.org/10.1021/acsami.9b17101
49. Meher N, Iyer PK (2019) Functional group engineering in naphthalimides: a conceptual insight to fine-tune the supramolecular self-assembly and condensed state luminescence. Nanoscale 11:13233–13242. https://doi.org/10.1039/C9NR04593G
50. Yang G, Liu L, Yang Q, Lv F, Wang S (2012) A Multifunctional Cationic Pentathiophene: Synthesis, Organelle-Selective Imaging, and Anticancer Activity. Adv Funct Mater 22:736–743. https://doi.org/10.1002/adfm.201101764
51. Jang SG, Audus DJ, Klinger D, Krogstad DV, Kim BJ, Cameron A, Kim SW, Delaney KT, Hur SM, Killops KL, Fredrickson GH, Kramer EJ, Hawker CJ (2013) Striped, Ellipsoidal Particles by Controlled Assembly of Diblock Copolymers. J Am Chem Soc 135:6649–6657. https://doi.org/10.1021/ja4019447
52. Hittinger E, Kokil A, Weder C (2004) Synthesis and Characterization of Cross-Linked Conjugated Polymer Milli-, Micro-, and Nanoparticles. Angew Chem Int Ed 116:1844–1847. https://doi.org/10.1002/ange.200352863
53. Müller K, Klapper M, Müllen K (2006) Synthesis of Conjugated Polymer Nanoparticles in Non-Aqueous Emulsions. Macromol Rapid Commun 27:586–593. https://doi.org/10.1002/marc.200600027
54. Jang J, Oh JH, Stucky GD (2002) Fabrication of Ultrafine Conducting Polymer and Graphite Nanoparticles. Angew Chem Int Ed 41:4016–4019. https://doi.org/10.1002/1521-3773(20021104)41:21%3c4016::AID-ANIE4016%3e3.0.CO;2-G
55. Mumtaz M, de Cuendias A, Putaux J-L, Cloutet E, Cramail H (2006) Synthesis of PEDOT Nanoparticles and Vesicles by Dispersion Polymerization in Alcoholic Media. Macromol Rapid Commun 27:1446–1453. https://doi.org/10.1002/marc.200600343
56. Mumtaz M, Lecommandoux S, Cloutet E, Cramail H (2008) Synthesis of Calibrated Poly(3,4-ethylenedioxythiophene) Latexes in Aqueous Dispersant Media. Langmuir 24:11911–11920. https://doi.org/10.1021/la801591d
57. Bremer LGB, Verbong MWCG, Webers MAM, van Doorn MAMM (1997) Preparation of core-shell dispersions with a low tg polymer core and a polyaniline shell. Synth Met 84:355–356. https://doi.org/10.1016/S0379-6779(97)80779-5
58. Wiersmavd Steeg , Jongeling AEL M AT J M (1995) Waterborne core-shell dispersions based on intrinsically conducting polymers for coating applications. Synth Met 71:2269–2270. https://doi.org/10.1016/0379-6779(94)03254-4
59. Barthet C, Armes SP, Chehimi MM, Bilem C, Omastova M (1998) Surface Characterization of Polyaniline-Coated Polystyrene Latexes. Langmuir 14:5032–5038. https://doi.org/10.1021/la980102r
60. Lascelles SF, Armes SP (1997) Synthesis and characterization of micrometre-sized, polypyrrole-coated polystyrene latexes. J Mater Chem 7:1339–1347. https://doi.org/10.1039/A700237H
61. Lascelles SF, Armes SP (1995) Synthesis and characterization of micrometersized polypyrrole-coated polystyrene latexes*. Adv Mater 7:864–866. https://doi.org/10.1002/adma.19950071011
62. Khan MA, Armes SP, Perruchot C, Ouamara H, Chehimi MM, Greaves SJ, Watts JF (2000) Surface Characterization of Poly(3,4-ethylenedioxythiophene)-Coated Latexes by X-ray Photoelectron Spectroscopy. Langmuir 16:4171–4179. https://doi.org/10.1021/la991390+
63. Kelly TL, Yamada Y, Che SPY, Yano K, Wolf MO (2008) Monodisperse Poly(3,4-ethylenedioxythiophene)–Silica Microspheres: Synthesis and Assembly into Crystalline Colloidal Arrays. Adv Mater 20:2616–2621. https://doi.org/10.1002/adma.200703131
64. Kelly TL, Yamada Y, Schneider C, Yano K, Wolf MO (2009) Enhanced Optical Properties and Opaline Self-Assembly of PPV Encapsulated in Mesoporous Silica Spheres. Adv Funct Mater 19:3737–3745. https://doi.org/10.1002/adfm.200901484
65. Kelly TL, Che SPY, Yamada Y, Yano K, Wolf MO (2008) Influence of Surface Morphology on the Colloidal and Electronic Behavior of Conjugated Polymer−Silica Microspheres. Langmuir 24:9809–9815. https://doi.org/10.1021/la8013688
66. Liu B, Bazan GC (2004) Interpolyelectrolyte Complexes of Conjugated Copolymers and DNA: Platforms for Multicolor Biosensors. J Am Chem Soc 126:1942–1943. https://doi.org/10.1021/ja038667j
67. Zhang SW, Swager TM (2003) Fluorescent Detection of Chemical Warfare Agents: Functional Group Specific Ratiometric Chemosensors. J Am Chem Soc 125:3420–3421. https://doi.org/10.1021/ja029265z
68. Yuan H, Qi J, Xing C, An H, Niu R, Zhan Y, Fan Y, Yan W, Li R, Wang B, Wang S (2015) Graphene-Oxide-Conjugated Polymer Hybrid Materials for Calmodulin Sensing by Using FRET Strategy. Adv Funct Mater 25:4412–4418. https://doi.org/10.1002/adfm.201501668
69. Wang X, Li S, Zhang P, Lv F, Liu L, Li L, Wang S (2015) An Optical Nanoruler Based on a Conjugated Polymer−Silver Nanoprism Pair for Label-Free Protein Detection. Adv Mater 27:6040–6045. https://doi.org/10.1002/adma.201502880
70. Fang Z, Pu KY, Liu B (2008) Asymmetric Fluorescence Quenching of Dual-Emissive Porphyrin-Containing Conjugated Polyelectrolytes for Naked-Eye Mercury Ion Detection. Macromolecules 41:8380–8387. https://doi.org/10.1021/ma801874z
71. Liang J, Li K, Liu B (2013) Visual sensing with conjugated polyelectrolytes. Chem Sci 4:1377–1394. https://doi.org/10.1039/C2SC21792A
72. Malik AH, Hussain S, Kalita A, Iyer PK (2015) Conjugated Polymer Nanoparticles for the Amplified Detection of Nitro-explosive Picric Acid on Multiple Platforms. ACS Appl Mater Interfaces 7:26968–26976. https://doi.org/10.1021/acsami.5b08068
73. Ponta H, Sherman L, Herrlich PA (2003) CD44: From adhesion molecules to signalling regulators. Nat Rev Mol Cell Biol 4:33–45. https://doi.org/10.1038/nrm1004
74. Ishimoto T, Nagano O, Yae T, Tamada M, Motohara T, Oshima H, Oshima M, Ikeda T, Asaba R, Yagi H, Masuko T, Shimizu T, Ishikawa T, Kai K, Takahashi E, Imamura Y, Baba Y, Ohmura M, Suematsu M, Baba H, Saya H (2011) CD44 Variant Regulates Redox Status in Cancer Cells by Stabilizing the xCT Subunit of

System xc- and Thereby Promotes Tumor Growth. Cancer Cell 19:387–400. https://doi.org/10.1016/j.ccr.2011.01.038
75. Cheng P, Miao Q, Li J, Huang J, Xie C, Pu K (2019) Unimolecular Chemo-fluoro-luminescent Reporter for Crosstalk-Free Duplex Imaging of Hepatotoxicity. J Am Chem Soc 141:10581–10584. https://doi.org/10.1021/jacs.9b02580
76. Huang Y, Yao X, Zhang R, Ouyang L, Jiang R, Liu X, Song C, Zhang G, Fan Q, Wang L, Huang W (2014) Cationic Conjugated Polymer/Fluoresceinamine-Hyaluronan Complex for Sensitive Fluorescence Detection of CD44 and Tumor-Targeted Cell Imaging. ACS Appl Mater Interfaces 6:19144–19153. https://doi.org/10.1021/am505113p
77. Choi KY, Chung H, Min KH, Yoon HY, Kim K, Park JH, Kwon IC, Jeong SY (2010) Self-assembled hyaluronic acid nanoparticles for active tumor targeting. Biomaterials 31:106–114. https://doi.org/10.1016/j.biomaterials.2009.09.030
78. Twomey M, Na Y, Roche Z, Mendez E, Panday N, HeJ MJH (2013) Fabrication of Core-Shell Nanoparticles via Controlled Aggregation of Semiflexible Conjugated Polymer and Hyaluronic Acid. Macromolecules 46:6374–6378. https://doi.org/10.1021/ma400996y
79. Chong H, Zhu C, Song J, Feng L, Yang Q, Liu L, Lv F, Wang S (2013) Preparation and Optical Property of New Fluorescent Nanoparticles. Macromol Rapid Commun 34:736–742. https://doi.org/10.1002/marc.201200755
80. Huang Y, Song C, Li H, Zhang R, Jiang R, Liu X, Zhang G, Fan Q, Wang L, Huang W (2015) Cationic Conjugated Polymer/Hyaluronan-Doxorubicin Complex for Sensitive Fluorescence Detection of Hyaluronidase and Tumor-Targeting Drug Delivery and Imaging. ACS Appl Mater Interfaces 7:21529–21537. https://doi.org/10.1021/acsami.5b06799
81. Han Y, Chen T, Li Y, Chen L, Wei L, Xiao L (2019) Single-Particle Enumeration-Based Sensitive Glutathione S-Transferase Assay with Fluorescent Conjugated Polymer Nanoparticle. Anal Chem 91:11146–11153. https://doi.org/10.1021/acs.analchem.9b01849
82. Wang S, Huang M, Hua J, Wei L, Lin S, Xiao L (2021) Digital counting of single semiconducting polymer nanoparticles for the detection of alkaline phosphatase. Nanoscale 13:4946–4955. https://doi.org/10.1039/D0NR09232K
83. Wang Q-b, Zhang C-j, Lu Q, Liu Z-e, Yao J-s, Zhang X (2020) A "turn-on" fluorescence platform of detection glutathione using MnO2 nanosheets quenched fluorescent conjugated polymer nanoparticles. Dyes Pigm 176:108189. https://doi.org/10.1016/j.dyepig.2020.108189
84. Yan S, Huang R, Wang C, Zhou Y, Wang J, FuB WX, Zhou X (2012) A Two-photon Fluorescent Probe for Intracellular Detection of Tyrosinase Activity. Chem-Asian J 7:2782–2785. https://doi.org/10.1002/asia.201200762
85. Sun J, Mei H, Wang S, Gao F (2016) Two-Photon Semiconducting Polymer Dots with Dual-Emission for Ratiometric Fluorescent Sensing and Bioimaging of Tyrosinase Activity. Anal Chem 88:7372–7377. https://doi.org/10.1021/acs.analchem.6b01929
86. Sun J, Chen N, Chen X, Zhang Q, Gao F (2019) Two-Photon Fluorescent Nanoprobe for Glutathione Sensing and Imaging in Living Cells and Zebrafish Using a Semiconducting Polymer Dots Hybrid with Dopamine and β-Cyclodextrin. Anal Chem 91:12414–12421. https://doi.org/10.1021/acs.analchem.9b03010
87. Nakamura M, Sanji T, Tanaka M (2011) Fluorometric Sensing of Biogenic Amines with Aggregation-Induced Emission-Active Tetraphenylethenes. Chem-Eur J 17:5344–5349. https://doi.org/10.1002/chem.201003285
88. Lehane L, Olley J (2000) Histamine fish poisoning revisited. Int J Food Microbiol 58:1–37. https://doi.org/10.1016/S0168-1605(00)00296-8
89. Fücker K, Meyer RA, Pietsch HP (1974) Dünnschichtelektrophoretische Bestimmung biogener Amine in Fisch und Fischprodukten im Zusammenhang mit Lebensmittelintoxikationen. Nahrung 18:663–669. https://doi.org/10.1002/food.19740180612
90. Shalaby AR (1996) Significance of biogenic amines to food safety and human health. Food Res Int 29:675–690. https://doi.org/10.1016/S0963-9969(96)00066-X
91. Bauza T, Blaise A, Daumas F, Cabanis JC (1995) Determination of biogenic amines and their precursor amino acids in wines of the Vallée du Rhône by high-performance liquid chromatography with precolumn derivatization and fluorimetric detection. J Chromatogr A 707:373–379. https://doi.org/10.1016/0021-9673(95)00318-H
92. Loukou Z, Zotou A (2003) Determination of biogenic amines as dansyl derivatives in alcoholic beverages by high-performance liquid chromatography with fluorimetric detection and characterization of the dansylated amines by liquid chromatography–atmospheric pressure chemical ionization mass pectrometry. J Chromatogr A 996:103–113. https://doi.org/10.1016/S0021-9673(03)00558-2
93. Önal A (2007) A review: Current analytical methods for the determination of biogenic amines in foods. Food Chem 103:1475–1486. https://doi.org/10.1016/j.foodchem.2006.08.028
94. Draisci R, Volpe G, Lucentini L, Cecilia A, Federico R, Palleschi G (1998) Determination of biogenic amines with an electrochemical biosensor and its application to salted anchovies. Food Chem 62:225–232. https://doi.org/10.1016/S0308-8146(97)00167-2
95. Sanches-Silva A, Rodríguez-Bernaldo de Quirós A, López-Hernández J, Paseiro-Losada P (2004) Comparison between high-performance liquid chromatography and gas chromatography methods for fatty acid identification and quantification in potato crisps. J Chromatogr A 1032:7–15. https://doi.org/10.1016/j.chroma.2003.11.012
96. Zhong H, Liu C, Ge W, Sun R, Huang F, Wang X (2017) Self-Assembled Conjugated Polymer/Chitosan-graft-Oleic Acid Micelles for Fast Visible Detection of Aliphatic Biogenic Amines by "Turn-On" FRET. ACS Appl Mater Interfaces 9:22875–22884. https://doi.org/10.1021/acsami.7b06168
97. Li J, Tian C, Yuan Y, Yang Z, Yin C, Jiang R, Song W, Li X, Lu X, Zhang L, Fan Q, Huang W (2015) A Water-Soluble Conjugated Polymer with Pendant Disulfide Linkages to PEG Chains: A Highly Efficient Ratiometric Probe with Solubility-Induced Fluorescence Conversion for Thiol Detection. Macromolecules 48:1017–1025. https://doi.org/10.1021/ma5021775
98. Cui Q, Yang Y, Yao C, Liu R, Li L (2016) Aggregation-Induced Energy Transfer of Conjugated Polymer Materials for ATP Sensing. ACS Appl Mater Interfaces 8:35578–35586. https://doi.org/10.1021/acsami.6b12525
99. Volkow ND, Fowler JS, Wang GJ, Swanson JM (2004) Dopamine in drug abuse and addiction: results from imaging studies and treatment implications. Mol Psychiatry 9:557–569. https://doi.org/10.1038/sj.mp.4001507
100. Chaudhury D, Walsh JJ, Friedman AK, Juarez B, Ku SM, Koo JW, Ferguson D, Tsai HC, Pomeranz L, Christoffel DJ, Nectow AR, Ekstrand M, Domingos A, Mazei-Robison MS, Mouzon E, Lobo MK, Neve RL, Friedman JM, Russo SJ, Deisseroth K, Nestler EJ, Han MH (2013) Rapid regulation of depression-related behaviours by control of midbrain dopamine neurons. Nature 493:532–536. https://doi.org/10.1038/nature11713
101. Chen Z, Zhang C, Zhou T, Ma H (2015) Gold nanoparticle based colorimetric probe for dopamine detection based on the interaction between dopamine and melamine. Microchim Acta 182:1003–1008. https://doi.org/10.1007/s00604-014-1417-0
102. Kim JH, Auerbach JM, Rodríguez-Gómez JA, Velasco I, Gavin D, Lumelsky N, Lee SH, Nguyen J, Sánchez-Pernaute R, Bankiewicz K, McKay R (2002) Dopamine neurons derived from

embryonic stem cells function in an animal model of Parkinson's disease. Nature 418:50–56. https://doi.org/10.1038/nature00900
103. Justice JB (1993) Quantitative microdialysis of neurotransmitters. J Neurosci Methods 48:263–276. https://doi.org/10.1016/0165-0270(93)90097-B
104. Qian CG, Zhu S, Feng PJ, Chen YL, Yu JC, Tang X, Liu Y, Shen QD (2015) Conjugated Polymer Nanoparticles for Fluorescence Imaging and Sensing of Neurotransmitter Dopamine in Living Cells and the Brains of Zebrafish Larvae. ACS Appl Mater Interfaces 7:18581–18589. https://doi.org/10.1021/acsami.5b04987
105. Koide Y, Urano Y, Hanaoka K, Terai T, Nagano T (2011) Development of an Si-Rhodamine-Based Far-Red to Near-Infrared Fluorescence Probe Selective for Hypochlorous Acid and Its Applications for Biological Imaging. J Am Chem Soc 133:5680–5682. https://doi.org/10.1021/ja111470n
106. Wang H, Li Y, Chen Y, Li L, Fang T, Tang Z (2015) Development of a conjugated polymer-based fluorescent probe for selective detection of HOCl. J Mater Chem C 3:5136–5140. https://doi.org/10.1039/C5TC00611B
107. Muthuraj B, Hussain S, Iyer PK (2013) A rapid and sensitive detection of ferritin at a nanomolar level and disruption of amyloid β fibrils using fluorescent conjugated polymer. Polym Chem 4:5096–5107. https://doi.org/10.1039/C3PY00680H
108. Feng L, Guo L, Wang X (2017) Preparation, properties and applications in cell imaging and ions detection of conjugated polymer nanoparticles with alcoxyl bonding fluorene core. Biosens Bioelectron 87:514–521. https://doi.org/10.1016/j.bios.2016.08.114
109. Gao Z-y, Zhang X, Xing S, Lu Q, Yao J-s, Liu Q-z, Qiao C-d, Xie R-x, Ding B (2019) Conjugated polymer nanoparticles based on carbazole for detecting ferric ion (III) with a large Stokes shift and high sensitivity and the application in cell imaging. Dyes Pigm 168:68–76. https://doi.org/10.1016/j.dyepig.2019.04.030
110. Braeken Y, Cheruku S, Ethirajan A, Maes W (2017) Conjugated Polymer Nanoparticles for Bioimaging. Materials 10:1420. https://doi.org/10.3390/ma10121420
111. Li K, Liu B (2014) Polymer-encapsulated organic nanoparticles for fluorescence and photoacoustic imaging. Chem Soc Rev 43:6570–6597. https://doi.org/10.1039/C4CS00014E
112. Feng G, Liu J, Liu R, Mao D, Tomczak N, Liu B (2017) Ultrasmall Conjugated Polymer Nanoparticles with High Specificity for Targeted Cancer Cell Imaging. Adv Sci 4:1600407. https://doi.org/10.1002/advs.201600407
113. Jiang Y, Cui D, Fang Y, Zhen X, Upputuri PK, Pramanik M, Ding D, Pu K (2017) Amphiphilic semiconducting polymer as multifunctional nanocarrier for fluorescence/photoacoustic imaging guided chemo-photothermal therapy. Biomaterials 145:168–177. https://doi.org/10.1016/j.biomaterials.2017.08.037
114. Liu J, Li K, Liu B (2015) Far-Red/Near-Infrared Conjugated Polymer Nanoparticles for Long-Term In Situ Monitoring of Liver Tumor Growth. Adv Sci 2:1500008. https://doi.org/10.1002/advs.201500008
115. Wang L, Zhao Q, Zhang Z, Lu Z, Zhao Y, Tang Y (2018) Fluorescent Conjugated Polymer/Quarternary Ammonium Salt Coassembly Nanoparticles: Applications in Highly Effective Antibacteria and Bioimaging. ACS Appl Bio Mater 1:1478–1486. https://doi.org/10.1021/acsabm.8b00422
116. KoralliNega PDA, Vagiaki LE, Pavlou A, Siskos MG, Dimitrakopoulou-Strauss A, Gregoriou V G, Chochos C L (2020) New conjugated polymer nanoparticles with high photoluminescence quantum yields for far-red and near infrared fluorescence bioimaging. Mater Chem Front 4:2357–2369. https://doi.org/10.1039/D0QM00195C
117. Li J, Rao J, Pu K (2018) Recent progress on semiconducting polymer nanoparticles for molecular imaging and cancer phototherapy. Biomaterials 155:217–235. https://doi.org/10.1016/j.biomaterials.2017.11.025
118. Xiong L, Shuhendler AJ, Rao J (2012) Self-luminescing BRET-FRET near-infrared dots for in vivo lymph-node mapping and tumour imaging. Nat Commun 3:1193. https://doi.org/10.1038/ncomms2197
119. Xu Q, Choi MJ, Kim G, Lee SH, Yoon J (2018) Development of a Selective Fluorescent Probe for Hypochlorous Acid Detection and Imaging. Bull Korean Chem Soc 39:1355–1356. https://doi.org/10.1002/bkcs.11614
120. Feng L, Liu L, Lv F, Bazan GC, Wang S (2014) Preparation and Biofunctionalization of Multicolor Conjugated Polymer Nanoparticles for Imaging and Detection of Tumor Cells. Adv Mater 26:3926–3930. https://doi.org/10.1002/adma.201305206
121. Morin JF, Leclerc M (2002) 2,7-Carbazole-Based Conjugated Polymers for Blue, Green, and Red Light Emission. Macromolecules 35:8413–8417. https://doi.org/10.1021/ma020880x
122. Feng X, Yang G, Liu L, Lv F, Yang Q, Wang S, Zhu D (2012) A Convenient Preparation of Multi-Spectral Microparticles by Bacteria-Mediated Assemblies of Conjugated Polymer Nanoparticles for Cell Imaging and Barcoding. Adv Mater 24:637–641. https://doi.org/10.1002/adma.201102026
123. Li S, Wang X, Hu R, Chen H, Li M, Wang J, Wang Y, Liu L, Lv F, Liang XJ, Wang S (2016) Near-Infrared (NIR)-Absorbing Conjugated Polymer Dots as Highly Effective Photothermal Materials for In Vivo Cancer Therapy. Chem Mater 28:8669–8675. https://doi.org/10.1021/acs.chemmater.6b03738
124. Ghani SM, Rezaei B, Jamei HR, Ensafi AA (2020) Preparation and comparison of molecularly imprinted polymer fluorimetric nanoprobe based on polymer dots and carbon quantum dots for determination of acetamiprid using response surface method. Microchim Acta 187:294. https://doi.org/10.1007/s00604-020-04283-x
125. Yu J, Wu C, Sahu SP, Fernando LP, Szymanski C, McNeill J (2009) Nanoscale 3D Tracking with Conjugated Polymer Nanoparticles. J Am Chem Soc 131:18410–18414. https://doi.org/10.1021/ja907228q
126. Chowdhury SR, Mukherjee S, Das S, Patra CR, Iyer PK (2017) Multifunctional (3-in-1) cancer theranostics applications of hydroxyquinoline-appended polyfluorene nanoparticles. Chem Sci 8:7566–7575. https://doi.org/10.1039/C7SC03321D
127. Koner AL, Krndija D, Hou Q, Sherratt DJ, Howarth M (2013) Hydroxy-Terminated Conjugated Polymer Nanoparticles Have Near-Unity Bright Fraction and Reveal Cholesterol-Dependence of IGF1R Nanodomains. ACS Nano 7:1137–1144. https://doi.org/10.1021/nn3042122
128. Zhang Y, Pang L, Ma C, Tu Q, Zhang R, Saeed E, Mahmoud AE, Wang J (2014) Small Molecule-Initiated Light-Activated Semiconducting Polymer Dots: An Integrated Nanoplatform for Targeted Photodynamic Therapy and Imaging of Cancer Cells. Anal Chem 86:3092–3099. https://doi.org/10.1021/ac404201s
129. Maestro LM, Ramírez-Hernández JE, Bogdan N, Capobianco JA, Vetrone F, Solé JG, Jaque D (2012) Deep tissue bio-imaging using two-photon excited CdTe fluorescent quantum dots working within the biological window. Nanoscale 4:298–302. https://doi.org/10.1039/C1NR11285F
130. Crosignani V, Jahid S, Dvornikov A, Gratton E (2014) Deep tissue imaging by enhanced photon collection. J Innovative Opt Health Sci 07:1450034. https://doi.org/10.1142/s1793545814500345
131. Yi M, Yang S, Peng ZY, Liu CH, Li JS, Zhong WW, Yang R, H WH, (2014) Two-Photon Graphene Oxide/Aptamer Nanosensing Conjugate for In Vitro or In Vivo Molecular Probing. Anal Chem 86:3548–3554. https://doi.org/10.1021/ac5000015

132. Hong G, Antaris AL, Dai H (2017) Near-infrared fluorophores for biomedical imaging. Nat Biomed Eng 1:0010. https://doi.org/10.1038/s41551-016-0010
133. Jin Y, Ye F, Zeigler M, Wu C, Chiu DT (2011) Near-Infrared Fluorescent Dye-Doped Semiconducting Polymer Dots. ACS Nano 5:1468–1475. https://doi.org/10.1021/nn103304m
134. Yuan L, Lin W, Zhao S, Gao W, Chen B, He L, Zhu S (2012) A Unique Approach to Development of Near-Infrared Fluorescent Sensors for in Vivo Imaging. J Am Chem Soc 134:13510–13523. https://doi.org/10.1021/ja305802v
135. Lv Y, Liu P, Ding H, Wu Y, Yan Y, Liu H, Wang X, Huang F, Zhao Y, Tian Z (2015) Conjugated Polymer-Based Hybrid Nanoparticles with Two-Photon Excitation and Near-Infrared Emission Features for Fluorescence Bioimaging within the Biological Window. ACS Appl Mater Interfaces 7:20640–20648. https://doi.org/10.1021/acsami.5b05150
136. Wu PJ, Kuo SY, Huang YC, Chen CP, Chan YH (2014) Polydiacetylene-Enclosed Near-Infrared Fluorescent Semiconducting Polymer Dots for Bioimaging and Sensing. Anal Chem 86:4831–4839. https://doi.org/10.1021/ac404237q
137. Frank RN (2004) Diabetic Retinopathy. N Engl J Med 350:48–58. https://doi.org/10.1056/NEJMra021678
138. Wang XD, Wolfbeis OS (2014) Optical methods for sensing and imaging oxygen: materials, spectroscopies and applications. Chem Soc Rev 43:3666–3761. https://doi.org/10.1039/C4CS00039K
139. Sakadžić S, Roussakis E, Yaseen MA, Mandeville ET, Srinivasan VJ, Arai K, Ruvinskaya S, Devor A, Lo EH, Vinogradov SA, Boas DA (2010) Two-photon high-resolution measurement of partial pressure of oxygen in cerebral vasculature and tissue. Nat Methods 7:755–759. https://doi.org/10.1038/nmeth.1490
140. Ma DL, He HZ, Zhong HJ, Lin S, Chan DSH, Wang L, Lee SMY, Leung CH, Wong CY (2014) Visualization of Zn2+ Ions in Live Zebrafish Using a Luminescent Iridium(III) Chemosensor. ACS Appl Mater Interfaces 6:14008–14015. https://doi.org/10.1021/am504369b
141. Zhao Q, Zhou X, Cao T, Zhang KY, Yang L, Liu S, Liang H, Yang H, Li F, Huang W (2015) Fluorescent/phosphorescent dual-emissive conjugated polymer dots for hypoxia bioimaging. Chem Sci 6:1825–1831. https://doi.org/10.1039/C4SC03062A
142. Siegel RL, Miller KD, Jemal A (2015) Cancer statistics, 2015. Ca-Cancer J Clin 65:5–29. https://doi.org/10.3322/caac.21254
143. Allaoui R, Bergenfelz C, Mohlin S, Hagerling C, Salari K, Werb Z, Anderson RL, Ethier SP, Jirström K, Påhlman S, Bexell D, Tahin B, Johansson ME, Larsson C, Leandersson K (2016) Cancer-associated fibroblast-secreted CXCL16 attracts monocytes to promote stroma activation in triple-negative breast cancers. Nat Commun 7:13050. https://doi.org/10.1038/ncomms13050
144. Khaled WT, Choon Lee S, Stingl J, Chen X, Raza Ali H, Rueda OM, Hadi F, Wang J, Yu Y, Chin SF, Stratton M, Futreal A, Jenkins NA, Aparicio S, Copeland NG, Watson CJ, Caldas C, Liu P (2015) BCL11A is a triple-negative breast cancer gene with critical functions in stem and progenitor cells. Nat Commun 6:5987. https://doi.org/10.1038/ncomms6987
145. Davies C, Pan H, Godwin J, Gray R, Arriagada R, Raina V, Abraham M, Alencar VHM, Badran A, Bonfill X, Bradbury J, Clarke M, Collins R, Davis SR, Delmestri A, Forbes JF, Haddad P, Hou MF, Inbar M, Khaled H, Kielanowska J, Kwan WH, Mathew BS, Mittra I, Müller B, Nicolucci A, Peralta O, Pernas F, Petruzelka L, Pienkowski T, Radhika R, Rajan B, Rubach MT, Tort S, Urrútia G, Valentini M, Wang Y, Peto R (2013) Long-term effects of continuing adjuvant tamoxifen to 10 years versus stopping at 5 years after diagnosis of oestrogen receptor-positive breast cancer: ATLAS, a randomised trial. Lancet 381:805–816. https://doi.org/10.1016/S0140-6736(12)61963-1
146. Jin G, He R, Liu Q, Dong Y, Lin M, Li W, Xu F (2018) Theranostics of Triple-Negative Breast Cancer Based on Conjugated Polymer Nanoparticles. ACS Appl Mater Interfaces 10:10634–10646. https://doi.org/10.1021/acsami.7b14603
147. Zhu C, Liu L, Yang Q, Lv F, Wang S (2012) Water-Soluble Conjugated Polymers for Imaging, Diagnosis, and Therapy. Chem Rev 112:4687–4735. https://doi.org/10.1021/cr200263w
148. Fruehauf JP, Meyskens FL (2007) Reactive Oxygen Species: A Breath of Life or Death? Clin Cancer Res 13:789. https://doi.org/10.1158/1078-0432.CCR-06-2082
149. Gorrini C, Harris IS, Mak TW (2013) Modulation of oxidative stress as an anticancer strategy. Nat Rev Drug Discovery 12:931–947. https://doi.org/10.1038/nrd4002
150. Li P, Liu L, Xiao H, Zhang W, Wang L, Tang B (2016) A New Polymer Nanoprobe Based on Chemiluminescence Resonance Energy Transfer for Ultrasensitive Imaging of Intrinsic Superoxide Anion in Mice. J Am Chem Soc 138:2893–2896. https://doi.org/10.1021/jacs.5b11784
151. Swager TM (1998) The Molecular Wire Approach to Sensory Signal Amplification. Acc Chem Res 31:201–207. https://doi.org/10.1021/ar9600502
152. Arias-Ramos N, Ibarra LE, Serrano-Torres M, Yagüe B, Caverzán MD, Chesta CA, Palacios RE, López-Larrubia P (2021) Iron Oxide Incorporated Conjugated Polymer Nanoparticles for Simultaneous Use in Magnetic Resonance and Fluorescent Imaging of Brain Tumors. Pharmaceutics 13:1258. https://doi.org/10.3390/pharmaceutics13081258
153. Palner M, Pu K, Shao S, Rao J (2015) Semiconducting Polymer Nanoparticles with Persistent Near-Infrared Luminescence for In Vivo Optical Imaging. Angew Chem Int Ed Engl 54:11477–11480. https://doi.org/10.1002/anie.201502736
154. Zhang J, Mohsin A, Peng Y, Dai Y, Zhuang Y, Guo M, Zhao P (2021) Sandwich-Type Near-Infrared Conjugated Polymer Nanoparticles for Revealing the Fate of Transplanted Human Umbilical Cord Mesenchymal Stem Cells. ACS Appl Mater Interfaces 13:3512–3520. https://doi.org/10.1021/acsami.0c13815
155. Song X, Lu X, Sun B, Zhang H, Sun P, Miao H, Fan Q, Huang W (2020) Conjugated Polymer Nanoparticles with Absorption beyond 1000 nm for NIR-II Fluorescence Imaging System Guided NIR-II Photothermal Therapy. ACS Appl Polym Mater 2:4171–4179. https://doi.org/10.1021/acsapm.0c00637
156. Ntziachristos V, Razansky D (2010) Molecular Imaging by Means of Multispectral Optoacoustic Tomography (MSOT). Chem Rev 110:2783–2794. https://doi.org/10.1021/cr9002566
157. Kim C, Favazza C, Wang LV (2010) In Vivo Photoacoustic Tomography of Chemicals: High-Resolution Functional and Molecular Optical Imaging at New Depths. Chem Rev 110:2756–2782. https://doi.org/10.1021/cr900266s
158. Pu K, Shuhendler AJ, Jokerst JV, Mei J, Gambhir SS, Bao Z, Rao J (2014) Semiconducting polymer nanoparticles as photoacoustic molecular imaging probes in living mice. Nat Nanotechnol 9:233–239. https://doi.org/10.1038/nnano.2013.302
159. Gao D, Zhang P, Liu Y, Sheng Z, Chen H, Yuan Z (2018) Protein-modified conjugated polymer nanoparticles with strong near-infrared absorption: a novel nanoplatform to design multifunctional nanoprobes for dual-modal photoacoustic and fluorescence imaging. Nanoscale 10:19742–19748. https://doi.org/10.1039/C8NR06197A
160. Li X, Kolemen S, Yoon J, Akkaya EU (2017) Activatable Photosensitizers: Agents for Selective Photodynamic Therapy. Adv Funct Mater 27:1604053. https://doi.org/10.1002/adfm.201604053
161. Wu W, Mao D, Xu S, Kenry HuF, Li X, Kong D, Liu B (2018) Polymerization-Enhanced Photosensitization. Chem 4:1937–1951. https://doi.org/10.1016/j.chempr.2018.06.003

162. Lovell JF, Liu TWB, Chen J, Zheng G (2010) Activatable Photosensitizers for Imaging and Therapy. Chem Rev 110:2839–2857. https://doi.org/10.1021/cr900236h
163. Cheng L, Wang C, Feng L, Yang K, Liu Z (2014) Functional Nanomaterials for Phototherapies of Cancer. Chem Rev 114:10869–10939. https://doi.org/10.1021/cr400532z
164. Nomoto T, Fukushima S, Kumagai M, Machitani K, Arnida MY, Oba M, Miyata K, Osada K, Nishiyama N, Kataoka K (2014) Three-layered polyplex micelle as a multifunctional nanocarrier platform for light-induced systemic gene transfer. Nat Commun 5:3545. https://doi.org/10.1038/ncomms4545
165. Cheng Y, Meyers JD, Broome AM, Kenney ME, Basilion JP, Burda C (2011) Deep Penetration of a PDT Drug into Tumors by Noncovalent Drug-Gold Nanoparticle Conjugates. J Am Chem Soc 133:2583–2591. https://doi.org/10.1021/ja108846h
166. Wang C, Cheng L, Liu Y, Wang X, Ma X, Deng Z, Li Y, Liu Z (2013) Imaging-Guided pH-Sensitive Photodynamic Therapy Using Charge Reversible Upconversion Nanoparticles under Near-Infrared Light. Adv Funct Mater 23:3077–3086. https://doi.org/10.1002/adfm.201202992
167. Huang P, Lin J, Wang X, Wang Z, Zhang C, He M, Wang K, Chen F, Li Z, Shen G, Cui D, Chen X (2012) Light-Triggered Theranostics Based on Photosensitizer-Conjugated Carbon Dots for Simultaneous Enhanced-Fluorescence Imaging and Photodynamic Therapy. Adv Mater 24:5104–5110. https://doi.org/10.1002/adma.201200650
168. Tu HL, Lin YS, Lin HY, Hung Y, Lo LW, Chen YF, Mou CY (2009) In vitro Studies of Functionalized Mesoporous Silica Nanoparticles for Photodynamic Therapy. Adv Mater 21:172–177. https://doi.org/10.1002/adma.200800548
169. Coll C, Bernardos A, Martínez-Máñez R, Sancenón F (2013) Gated Silica Mesoporous Supports for Controlled Release and Signaling Applications. Acc Chem Res 46:339–349. https://doi.org/10.1021/ar3001469
170. Wang Y, Wang K, Zhao J, Liu X, Bu J, Yan X, Huang R (2013) Multifunctional Mesoporous Silica-Coated Graphene Nanosheet Used for Chemo-Photothermal Synergistic Targeted Therapy of Glioma. J Am Chem Soc 135:4799–4804. https://doi.org/10.1021/ja312221g
171. Dong K, Liu Z, Li Z, Ren J, Qu X (2013) Hydrophobic Anticancer Drug Delivery by a 980 nm Laser-Driven Photothermal Vehicle for Efficient Synergistic Therapy of Cancer Cells In Vivo. Adv Mater 25:4452–4458. https://doi.org/10.1002/adma.201301232
172. Zhang Z, Wang L, Wang J, Jiang X, Li X, Hu Z, Ji Y, Wu X, Chen C (2012) Mesoporous Silica-Coated Gold Nanorods as a Light-Mediated Multifunctional Theranostic Platform for Cancer Treatment. Adv Mater 24:1418–1423. https://doi.org/10.1002/adma.201104714
173. Wang B, Yuan H, Liu Z, Nie C, Liu L, Lv F, Wang Y, Wang S (2014) Cationic Oligo(p-phenylene vinylene) Materials for Combating Drug Resistance of Cancer Cells by Light Manipulation. Adv Mater 26:5986–5990. https://doi.org/10.1002/adma.201402183
174. Qian C, Yu J, Chen Y, Hu Q, Xiao X, Sun W, Wang C, Feng P, Shen QD, Gu Z (2016) Light-Activated Hypoxia-Responsive Nanocarriers for Enhanced Anticancer Therapy. Adv Mater 28:3313–3320. https://doi.org/10.1002/adma.201505869
175. Zhao M, Leggett E, Bourke S, Poursanidou S, Carter-Searjeant S, Po S, Palma do Carmo M, Dailey L A, Manning P, Ryan S G, Urbano L, Green M A, Rakovich A (2021) Theranostic Near-Infrared-Active Conjugated Polymer Nanoparticles. ACS Nano 15:8790–8802. https://doi.org/10.1021/acsnano.1c01257
176. Zhou S, Wang Z, Wang Y, Feng L (2020) Near-Infrared Light-Triggered Synergistic Phototherapy for Antimicrobial Therapy. ACS Appl Bio Mater 3:1730–1737. https://doi.org/10.1021/acsabm.0c00034
177. Zhou S, Yang C, Guo L, Wang Y, Zhang G, Feng L (2019) Water-soluble conjugated polymer with near-infrared absorption for synergistic tumor therapy using photothermal and photodynamic activity. Chem Commun 55:8615–8618. https://doi.org/10.1039/C9CC03744F
178. Li J, Yu X, Jiang Y, He S, Zhang Y, Luo Y, Pu K (2021) Second Near-Infrared Photothermal Semiconducting Polymer Nanoadjuvant for Enhanced Cancer Immunotherapy. Adv Mater 33:2003458. https://doi.org/10.1002/adma.202003458
179. Huang X, El-Sayed IH, Qian W, El-Sayed MA (2006) Cancer Cell Imaging and Photothermal Therapy in the Near-Infrared Region by Using Gold Nanorods. J Am Chem Soc 128:2115–2120. https://doi.org/10.1021/ja057254a
180. Chen Q, Liang C, Wang X, He J, Li Y, Liu Z (2014) An albumin-based theranostic nano-agent for dual-modal imaging guided photothermal therapy to inhibit lymphatic metastasis of cancer post surgery. Biomaterials 35:9355–9362. https://doi.org/10.1016/j.biomaterials.2014.07.062
181. Song X, Zhang R, Liang C, Chen Q, Gong H, Liu Z (2015) Nanoassemblies of J-aggregates based on a NIR dye as a multifunctional drug carrier for combination cancer therapy. Biomaterials 57:84–92. https://doi.org/10.1016/j.biomaterials.2015.04.001
182. Jiang BP, Zhang L, Zhu Y, Shen XC, Ji SC, Tan XY, Cheng L, Liang H (2015) Water-soluble hyaluronic acid–hybridized polyaniline nanoparticles for effectively targeted photothermal therapy. J Mater Chem B 3:3767–3776. https://doi.org/10.1039/C4TB01738B
183. Su Z, Yang C, Xu C, Wu H, Zhang Z, Liu T, Zhang C, Yang Q, Li B, Kang F (2013) Co-electro-deposition of the MnO2–PEDOT:PSS nanostructured composite for high areal mass, flexible asymmetric supercapacitor devices. J Mater Chem A 1:12432–12440. https://doi.org/10.1039/C3TA13148C
184. Sun H, Lv F, Liu L, Gu Q, Wang S (2018) Conjugated Polymer Materials for Photothermal Therapy. Adv Ther 1:1800057. https://doi.org/10.1002/adtp.201800057
185. Roper DK, Ahn W, Hoepfner M (2007) Microscale Heat Transfer Transduced by Surface Plasmon Resonant Gold Nanoparticles. J Phys Chem C 111:3636–3641. https://doi.org/10.1021/jp064341w
186. Xu L, Cheng L, Wang C, Peng R, Liu Z (2014) Conjugated polymers for photothermal therapy of cancer. Polym Chem 5:1573–1580. https://doi.org/10.1039/C3PY01196H
187. Guo B, Feng G, Manghnani PN, Cai X, Liu J, Wu W, Xu S, Cheng X, Teh C, Liu B (2016) A Porphyrin-Based Conjugated Polymer for Highly Efficient In Vitro and In Vivo Photothermal Therapy. Small 12:6243–6254. https://doi.org/10.1002/smll.201602293
188. Yi X, Yang K, Liang C, Zhong X, Ning P, Song G, Wang D, Ge C, Chen C, Chai Z, Liu Z (2015) Imaging-Guided Combined Photothermal and Radiotherapy to Treat Subcutaneous and Metastatic Tumors Using Iodine-131-Doped Copper Sulfide Nanoparticles. Adv Funct Mater 25:4689–4699. https://doi.org/10.1002/adfm.201502003
189. Zhou M, Chen Y, Adachi M, Wen X, Erwin B, Mawlawi O, Lai SY, Li C (2015) Single agent nanoparticle for radiotherapy and radio-photothermal therapy in anaplastic thyroid cancer. Biomaterials 57:41–49. https://doi.org/10.1016/j.biomaterials.2015.04.013
190. Yong Y, Cheng X, Bao T, Zu M, Yan L, Yin W, Ge C, Wang D, Gu Z, Zhao Y (2015) Tungsten Sulfide Quantum Dots as Multifunctional Nanotheranostics for In Vivo Dual-Modal Image-Guided Photothermal/Radiotherapy Synergistic Therapy. ACS Nano 9:12451–12463. https://doi.org/10.1021/acsnano.5b05825

191. Guo B, Sheng Z, Hu D, Li A, Xu S, Manghnani PN, Liu C, Guo L, Zheng H, Liu B (2017) Molecular Engineering of Conjugated Polymers for Biocompatible Organic Nanoparticles with Highly Efficient Photoacoustic and Photothermal Performance in Cancer Theranostics. ACS Nano 11:10124–10134. https://doi.org/10.1021/acsnano.7b04685
192. Wang Y, Li S, Zhang P, Bai H, Feng L, Lv F, Liu L, Wang S (2018) Photothermal-Responsive Conjugated Polymer Nanoparticles for Remote Control of Gene Expression in Living Cells. Adv Mater 30:1705418. https://doi.org/10.1002/adma.201705418
193. Geng J, Sun C, Liu J, Liao LD, Yuan Y, Thakor N, Wang J, Liu B (2015) Biocompatible Conjugated Polymer Nanoparticles for Efficient Photothermal Tumor Therapy. Small 11:1603–1610. https://doi.org/10.1002/smll.201402092
194. Zhen X, Xie C, Pu K (2018) Temperature-Correlated Afterglow of a Semiconducting Polymer Nanococktail for Imaging-Guided Photothermal Therapy. Angew Chem Int Ed 57:3938–3942. https://doi.org/10.1002/anie.201712550
195. Sun T, Han J, Liu S, Wang X, Wang ZY, Xie Z (2019) Tailor-Made Semiconducting Polymers for Second Near-Infrared Photothermal Therapy of Orthotopic Liver Cancer. ACS Nano 13:7345–7354. https://doi.org/10.1021/acsnano.9b03910
196. Sun T, Dou JH, Liu S, Wang X, Zheng X, Wang Y, Pei J, Xie Z (2018) Second Near-Infrared Conjugated Polymer Nanoparticles for Photoacoustic Imaging and Photothermal Therapy. ACS Appl Mater Interfaces 10:7919–7926. https://doi.org/10.1021/acsami.8b01458
197. Cao Y, Dou JH, Zhao NJ, Zhang S, Zheng YQ, Zhang JP, Wang JY, Pei J, Wang Y (2017) Highly Efficient NIR-II Photothermal Conversion Based on an Organic Conjugated Polymer. Chem Mater 29:718–725. https://doi.org/10.1021/acs.chemmater.6b04405
198. Xu C, Pu K (2021) Second near-infrared photothermal materials for combinational nanotheranostics. Chem Soc Rev 50:1111–1137. https://doi.org/10.1039/D0CS00664E
199. Wei Z, Zhu B, Cai Y, Yan D, Lou Y, Guo Z, Deng P (2020) Near-Infrared-Absorbing Diketopyrrolopyrrole-Based Semiconducting Polymer Nanoparticles for Photothermal Therapy. Part Part Syst Charact 37:1900433. https://doi.org/10.1002/ppsc.201900433
200. Cheng X, Sun R, Yin L, Chai Z, Shi H, Gao M (2017) Light-Triggered Assembly of Gold Nanoparticles for Photothermal Therapy and Photoacoustic Imaging of Tumors In Vivo. Adv Mater 29:1604894. https://doi.org/10.1002/adma.201604894
201. Smith AM, Mancini MC, Nie S (2009) Second window for in vivo imaging. Nat Nanotechnol 4:710–711. https://doi.org/10.1038/nnano.2009.326
202. Feng X, Lv F, Liu L, Tang H, Xing C, Yang Q, Wang S (2010) Conjugated Polymer Nanoparticles for Drug Delivery and Imaging. ACS Appl Mater Interfaces 2:2429–2435. https://doi.org/10.1021/am100435k
203. Lee MH, Thomas JL, Chen YC, Chin WT, Lin HY (2013) The complete replacement of antibodies by protein-imprinted poly (ethylene-co-vinyl alcohol) in sandwich fluoroimmunoassays. Microchim Acta 180:1393–1399. https://doi.org/10.1007/s00604-013-0995-6
204. Peer D, Karp JM, Hong S, Farokhzad OC, Margalit R, Langer R (2007) Nanocarriers as an emerging platform for cancer therapy. Nat Nanotechnol 2:751–760. https://doi.org/10.1038/nnano.2007.387
205. Xu X, Liu R, Li L (2015) Nanoparticles made of π-conjugated compounds targeted for chemical and biological applications. Chem Commun 51:16733–16749. https://doi.org/10.1039/C5CC06439B
206. Elsabahy M, Heo GS, Lim SM, Sun G, Wooley KL (2015) Polymeric Nanostructures for Imaging and Therapy. Chem Rev 115:10967–11011. https://doi.org/10.1021/acs.chemrev.5b00135
207. Senthilkumar T, Zhou L, Gu Q, Liu L, Lv F, Wang S (2018) Conjugated Polymer Nanoparticles with Appended Photo-Responsive Units for Controlled Drug Delivery, Release, and Imaging. Angew Chem Int Ed 57:13114–13119. https://doi.org/10.1002/anie.201807158
208. Lu Z, Zhang Z, Tang Y (2019) Conjugated Polymers-Based Thermal-Responsive Nanoparticles for Controlled Drug Delivery, Tracking, and Synergistic Photodynamic Therapy/Chemotherapy. ACS Appl Bio Mater 2:4485–4492. https://doi.org/10.1021/acsabm.9b00640